

ACE Deliverable 2.2-D8

Antenna Technology for Reconfigurable Multiple Antenna Terminals

Project Number: FP6-IST 508009
Project Title: Antenna Centre of Excellence
Document Type: Deliverable

Document Number: *FP6-IST 508009/2.2D8*

Contractual date of delivery: *31st December 2005*

Actual date of delivery: *31st December 2005*

Workpackage: *WP2.2-3*

Security : *Public*

Nature: *Report*

Editor(s): *Björn Lindmark (KTH), Monica Navarro(CTTC)*

Author (s): *Björn Lindmark (KTH), Niklas Jaldén (KTH), Per Zetterberg (KTH), Laura Garcia-Garcia (UPM), T. Zervos (NCSRD), A. Alexandridis (NCSRD), Fotis Lazarakis (NCSRD), K. Dangakis (NCSRD), Charlie Orlenius (CHALMERS), Magnus Franzén (CHALMERS).*

Participant(s): *KTH, UPM, CHALMERS, NCSRD.*

Abstract: Study of the performance of two different MIMO antenna arrays for mobile communications using channel measurements, radiation patterns, and a reverberation chamber are presented as part of the integrating research activities that have taken place within WP2.2-3 framework .

Keyword list: MIMO antenna arrays, channel measurements, antenna technology, human body effects.

Table of Contents

EXECUTIVE SUMMARY	3
1 INTRODUCTION	4
1.1 TIMELINE OF THE WORK DONE IN WP 2.2-3, TASK 5:.....	4
1.2 JOINT WORK AND PUBLICATIONS	5
2 DESIGN OF RE-CONFIGURABLE ANTENNAS AND ELEMENTS FOR MULTIPLE ANTENNA SYSTEMS.....	5
2.1 EXAMPLE OF A COMPACT ANTENNA ARRAY	6
3 MODELING, CHARACTERIZATION AND MEASUREMENT OF MULTIPLE ANTENNA SYSTEMS.....	8
3.1 EVALUATION BASED ON PATTERNS ALONE	8
3.2 REVERBERATION CHAMBER MEASUREMENTS AT CHALMERS.....	9
3.3 CHANNEL MEASUREMENTS AT KTH.....	11
3.3.1 <i>Example 1: Hallway LOS, 4th floor, route 1 →4</i>	13
3.3.2 <i>Example 2: Hallway NLOS, 5th floor, route 4 →8</i>	17
3.3.3 <i>Example 3: Office-like environment, 4th floor, Conference room</i>	22
4 THE EFFECT OF THE HUMAN BODY.....	26
4.1 AUT IN HAND	26
4.2 AUT ON BODY	33
4.3 RESULTS	36
5 CONCLUSION AND DISCUSSION	37
REFERENCES BY MEMBERS OF ACE	38
OTHER REFERENCES.....	38
ACRONYMS/TERMINOLOGY	40

Executive Summary

This deliverable summarizes the work done in Task 5 of WP 2.2-3 on antenna aspects of MIMO systems in mobile communications. The focus of this task within the framework of WP2.2-3 on reconfigurable/advanced MIMO transceivers is on the antenna technology aspects. This activity has gathered the expertise on antenna design and measurement issues applied to MIMO systems. The integration of the research addressed in this task has been very successful, where three partners have been closely working towards the design of two antenna reference sets for MIMO characterization as compare to theoretical results. The execution of the joint research activities implied sharing measurement facilities and data among partners.

The work was organized around three items: the design of a compact antenna array operating at 1766 MHz and 2450 MHz suited for a hand-held device in a MIMO system, the evaluation of this array and a reference monopole array using three different simulation and measurement methods, and a numerical study of the effect of the human body on the performance.

We find that all investigated methods lead to a similar result. The compact antennas array provides a slightly worse MIMO performance which may be attributed to its lower radiation efficiency. The difference is, however, rather small.

1 Introduction

The performance of a MIMO system depends on a number of factors including the propagation conditions, the type of signalling used, and the amount of feedback from receiver to transmitter [1]. However, it is also strongly dependent on the antenna arrays used and how well suited they are to the propagation conditions at hand. While the original contribution to multiple antenna and MIMO systems have come from communication or signal processing, we have recently seen an increased interest from the antenna and electromagnetic community to investigate how the antennas affect the system performance.

In fact, some of the fundamental work in the area date back to the 60's and 70's when fundamental array theory was used to investigate how the efficiency of a multi-antenna system is reduced from mutual coupling. In particular, it was shown in [13] that the peak gain of a two-element array cannot be increased by using a small spacing because any increased directivity is lost in mutual coupling losses. More recently, [14] investigated how mutual coupling can decrease antenna correlation and thus increase capacity in MIMO systems. However, if one also accounts for losses from impedance mismatch and mutual coupling, the overall effect of closely spaced elements with mutual coupling is to reduce the available capacity [1],[4],[6],[15]. The polarization and radiation pattern of the antennas may also influence the MIMO performance if the radio propagation results in a incident field which is not isotropic and of random polarization [2], [3],[16]. Yet another aspect of MIMO arrays is the possibility of *re-configuring* the antenna elements to better suit a certain radio channel realization. This will be discussed further in Sect. 3.1 below.

Since antenna arrays affect the theoretical MIMO capacity, it is of interest to be able to evaluate them in an efficient and accurate way. In WP 2.2-3, Task 5, we have studied three ways to evaluate MIMO antenna arrays:

- Capacity simulations using radio channel data collected for the antenna array in question [8]
- Capacity simulation using the measured radiation patterns and a theoretical channel model [19]
- Capacity simulations using a reverberation chamber [6]

The first method is clearly the ideal way to evaluate any antenna, but it is very time-consuming and also brings up some questions on which environment should be used in the evaluation. The second approach is certainly less time-consuming, but it calls for knowledge of the full 2-D radiation pattern in azimuth and elevation as in e.g. [2]. The third approach circumvents the need for time-consuming channel measurements or 2-D radiation pattern data, but is less flexible in the type of radio channels that may be used in the evaluation.

In this task we have studied the MIMO capacity performance of a compact antenna array, *antenna under test* (AUT), for mobile communications and WLAN applications. The MIMO system performance of the antenna array is compared to the performance of a *reference array* (REF) with 4 vertical monopoles.

Finally, the above antenna evaluations concern antennas in free space, but it is clear that many applications will see antenna arrays at one end of the link, i.e. the user terminal, in the vicinity of the human body. The work concentrates on evaluating the increased losses and antenna mismatch caused by the human body. Section 5 presents numerical simulations of the AUT near a human body and the implications for a MIMO system.

1.1 Timeline of the work done in WP 2.2-3, Task 5:

CAD of antenna array on model of device	KTH/UPM	April-May 2005
Design and manufacture of reference antenna	KTH	June 2005
Simulation of case antennas in the vicinity of the human body	NCSRD	May-Sept. 2005
Manufacture of compact antenna array	KTH	June 2005

CST files sent to NCSR	KTH/UPM	July 2005
MIMO measurements using test-bed	KTH/UPM	July 2005
Measurements of radiation patterns	KTH	Sept. 2005
Simulations of capacity	KTH	Aug.-Nov. 2005
Measurements in reverberation chamber	CHALMERS	Nov. 2005

1.2 Joint work and publications

From the previous section it is evident that behind this deliverable has been a collaborative effort of 4 partners from Sweden, Spain, and Greece. In addition, the work will be disseminated through the following planned joint publications:

- 1) “Compact antenna array for MIMO applications at 1800 and 2450 MHz”, Laura Garcia-Garcia (UPM), Niklas Jaldén (KTH), Björn Lindmark (KTH), submitted to IEEE Antenna and Wireless Propagation Letters, Dec. 2005.
- 2) "Indoor MIMO channel capacity using different indoor and outdoor transmitter locations" Laura Garcia-Garcia (UPM), Niklas Jaldén (KTH), Björn Lindmark (KTH), to be submitted to EURASIP J. Wireless Communications and Networking, 2006
- 3) "Evaluation of different MIMO arrays using EM simulation, channel measurements, and propagation modelling", Laura Garcia-Garcia (UPM), Björn Lindmark (KTH) , Niklas Jaldén (KTH) Charlie Orlenius (CHALMERS), to be submitted to IEEE Trans. Antennas Propagat., 2006.

2 Design of re-configurable antennas and elements for multiple antenna systems

Re-configurable antennas can be made for different frequencies, patterns, polarization, or a combination of the above [25][26][27][28][29][30][31]. Shifting frequency may be used in a re-configurable MIMO system, but is perhaps of less interest since most systems have a fixed and rather narrow bandwidth. It is therefore possible to shift frequency of the link without changing the antenna. Change of polarization or radiation pattern is of greater interest. An example of such a design is seen in Fig. 1 below. This work will be extended to real-time tests in ACE-2. This deliverable will focus on the performance of different fixed antenna arrays.

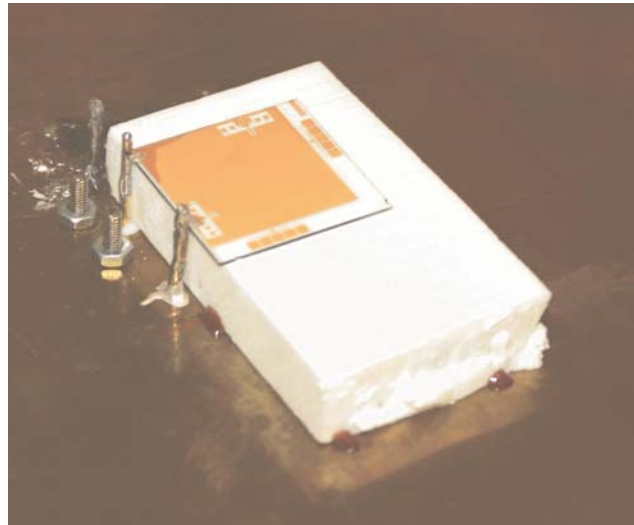


Fig. 1: Photograph of a reconfigurable antenna element for 1766 MHz where a square patch element is fed by a coaxial line at the corner and the polarization determined by grounding in one of two different locations. The location is in this case to be made using RF-MEMS switches (not shown). The size of the patch is 20 x 20 mm.

2.1 Example of a compact antenna array

In order to compare different methods of evaluating MIMO antenna arrays, we have designed the arrays shown in Fig. 2. The left array, here referred to as the *compact antenna array* or the *antenna under test* (AUT), consists of 4 antenna elements, designed for operation at 1766 MHz and 2450 MHz. The elements are folded PIFA patch elements as described in [31]. The array was designed under the constraint that the elements would fit on 75 x 75 mm² or on a 75 x 125 mm² large PDA dummy. Similar antenna designs for mobile multi-antenna application may be found in [5][21][22][24].

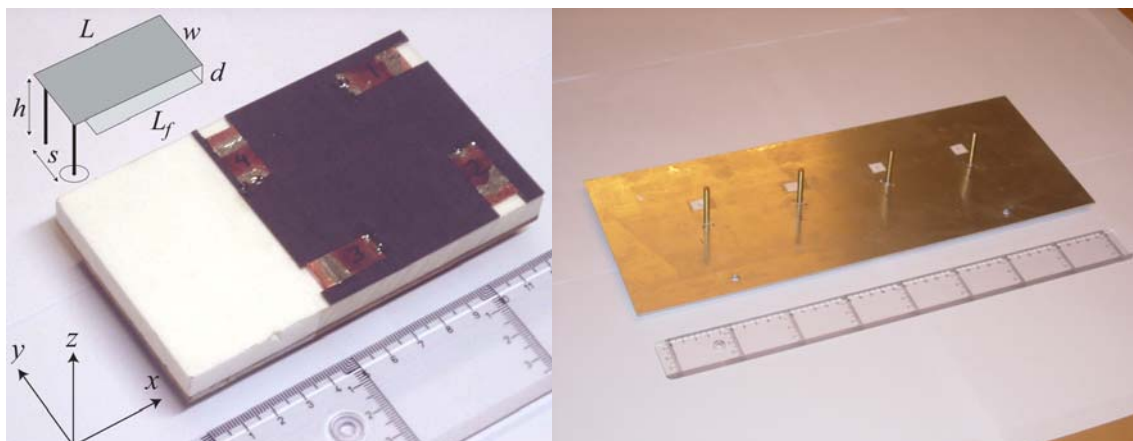


Fig. 2 : Photograph of the compact array, or AUT, with a drawing of the elements (left), and the reference monopole array REF (right).

The other antenna, shown in the right hand side of Fig. 2 and referred to as the *reference array* (REF), consists of 4 parallel monopoles with a center frequency of 1766 MHz placed with $\lambda/2$ spacing on a $5/2 \lambda \times 1\lambda$ ground plane. In the design of the compact array, an important issue is the level of mutual coupling between the elements. Although mutual coupling may reduce element correlation due to the resulting different patterns [14], it is also known that the overall effect is detrimental [1],[4],[15]. Furthermore, if the arrays are used in radio channel measurement, it is difficult to accurately control the amount of radiated

power if the mutual coupling or reflection is too high. We therefore analyzed the three different configurations shown in the left hand side of Fig. 3. The first setting has the elements sequentially rotated and being images of each other, the second has the elements parallel and polarized along the y -axis, and the third has the elements parallel and polarized along the x -axis. On the right hand side of Fig. 3 it is shown the limiting coupling coefficients, i.e. the highest values, from which it is clear that the second configuration leads to a very high coupling of around -8 dB between two of the closest elements. The first and third ones are quite similar. Thus we chose the first design since we expect it to provide lower correlation due to the greater differences between element polarization.

The antenna was then built and measured and the results are shown in Figs. 4-5. The agreement between simulated and measured S-parameters is quite good, as seen in Fig. 4. The radiation pattern was measured in the 2D Satimo chamber of AMC Centurion, Åkersberga, Sweden. We can see that the maxima and minima are different for the 4 antennas depending on their position on the PDA dummy, but that all elements have fairly omni-directional patterns in the horizontal plane ($\theta = 90^\circ$).

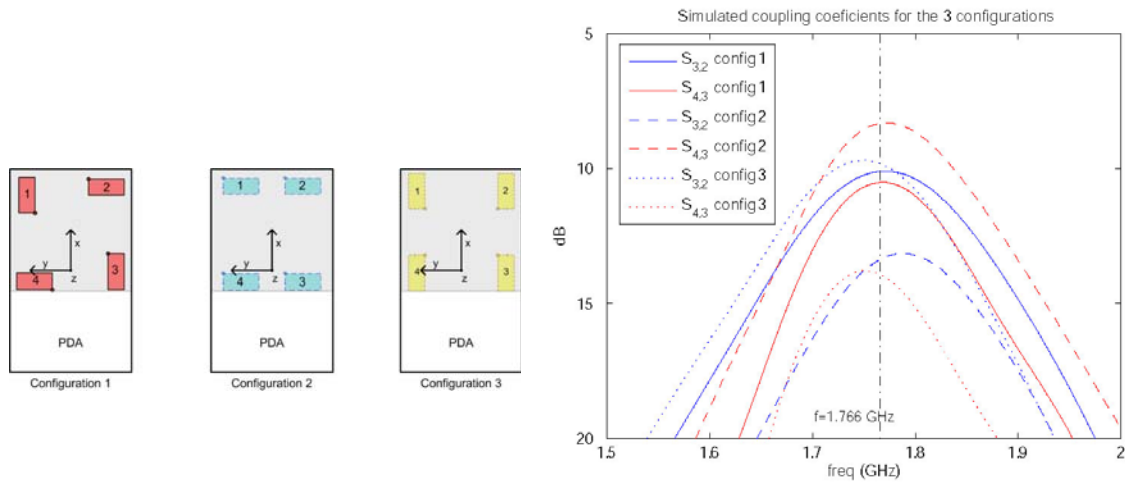


Fig. 3: Three different element configuration and the simulated mutual coupling between the elements for each case.

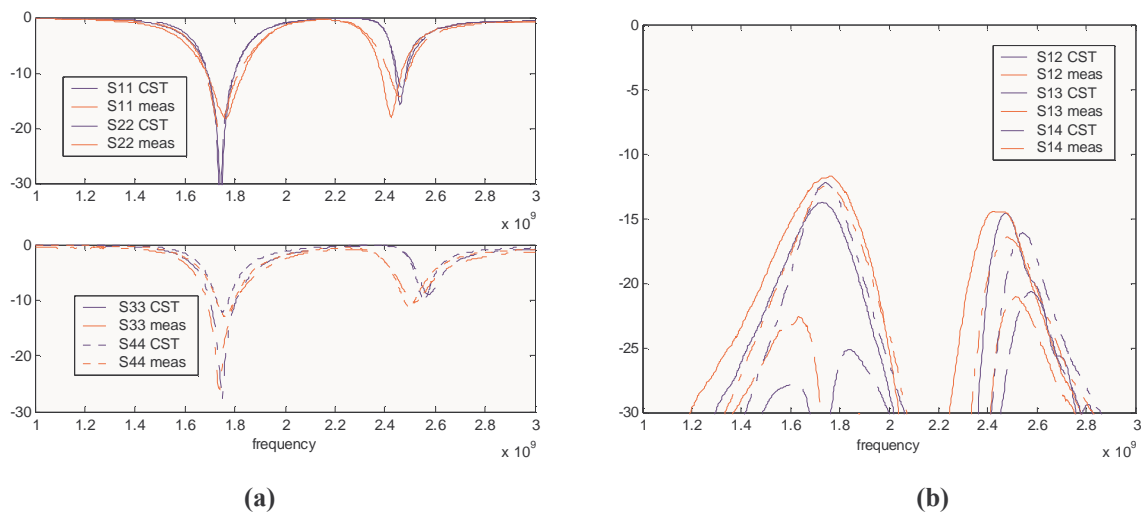


Fig. 4: Simulated and measured scattering parameters for the 4 ports of the compact antenna array (AUT). (a) Reflection coefficients (b) mutual coupling.

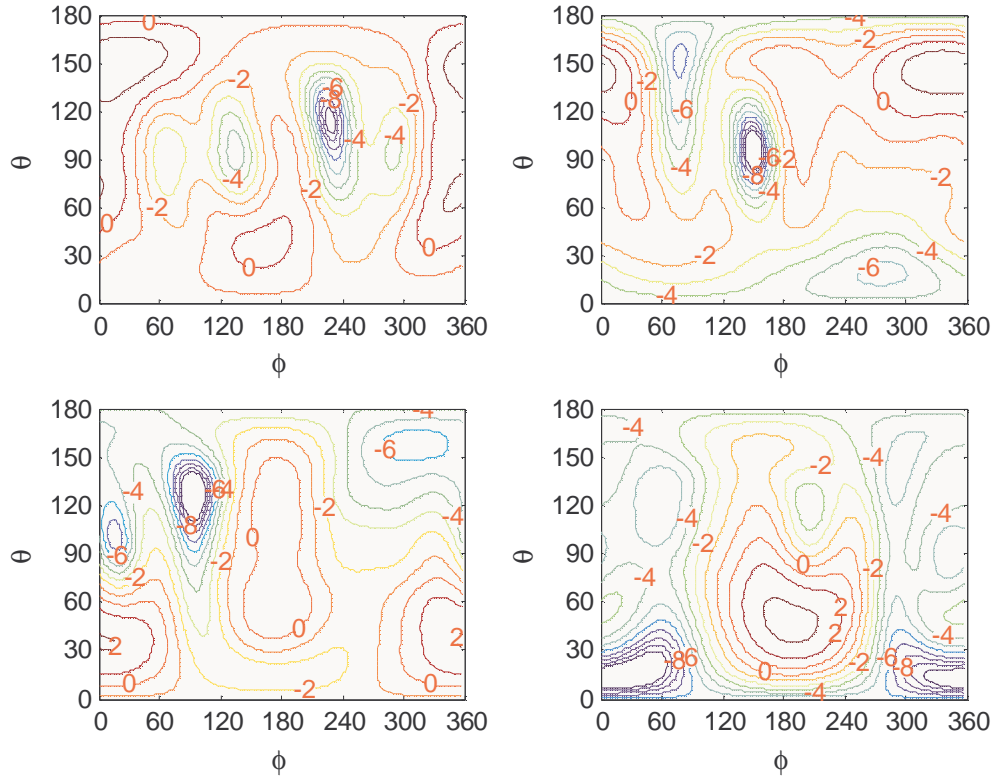


Fig. 5. Measured antenna gain in dB of the 4 elements of the compact antenna array (AUT).

3 Modeling, characterization and measurement of multiple antenna systems

3.1 Evaluation based on patterns alone

It is possible to estimate the MIMO performance of an antenna array based on the radiation patterns alone if sufficient simplifications of the radio channel are made. In particular, the so-called Kronecker model is particularly attractive since it allows us to separate the effects caused by the arrays at each end of the link. The well-known theoretical MIMO capacity C is given by,

$$C = \log_2 \det[I_{n_R} + (\rho/n_T)\mathbf{H}\mathbf{H}^H]$$

where ρ is the average signal-to-noise ratio (SNR) at each receiver and \mathbf{H} denotes the channel matrix. In the Kronecker model, the channel \mathbf{H} is related to the covariance of the signals at receive and transmit ends by,

$$\mathbf{H} = 1/g (\mathbf{R}_{rx})^{1/2} \mathbf{G} (\mathbf{R}_{tx}^T)^{1/2}$$

where \mathbf{G} is a random complex Gaussian matrix and g a normalization constant to achieve the desired SNR ρ . The elements of the covariance matrix are determined by the radiation patterns \mathbf{E}_i and \mathbf{E}_j . With an appropriate normalization of the radiation patterns so that $R(i,i) = 1$ for a loss-less antenna, we may follow [4],[17] and define:

$$R_{rx}(i,j) = R_{tx}(i,j) = \iint_{\Omega} \mathbf{E}_i \cdot \mathbf{E}_j^* d\Omega$$

Thus, to compare the arrays AUT and REF we only need to study their radiation patterns and the associated covariance matrix of each array. Fig. 6 below shows the absolute value of the different covariance coefficients for different incident field distributions. It is clear that the variation of the covariance is small, and that the main difference between the arrays lies in the radiation efficiency associated to the variance.

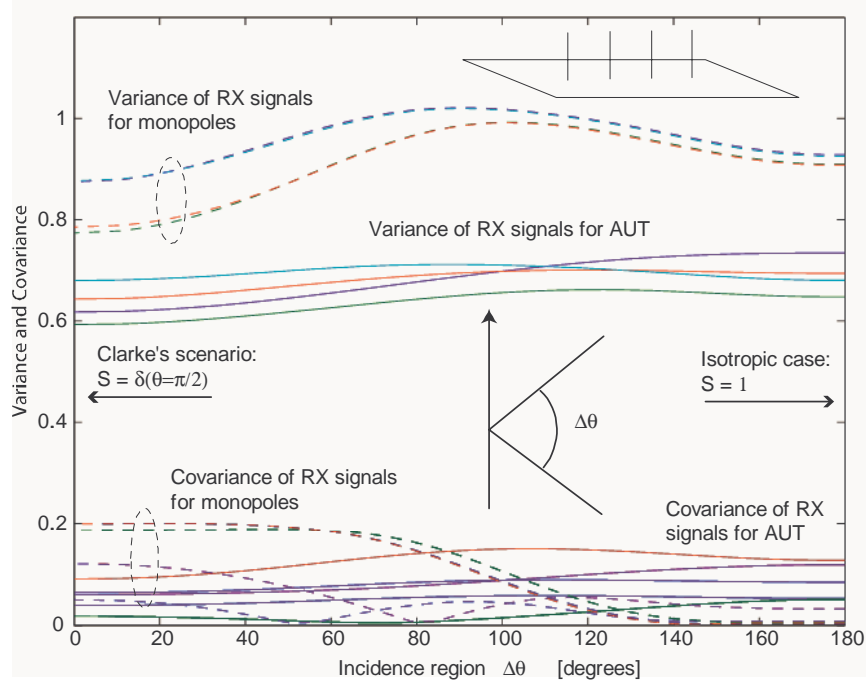


Fig. 6: Covariance between antenna ports normalized so that a loss-less antenna has a variance of 1 at $\Delta\theta = 180^\circ$ (isotropic incidence). The variance value on the far right is therefore equal to the radiation efficiency.

3.2 Reverberation chamber measurements at CHALMERS

As an alternative to time-consuming channel measurements, a uniform multi-path environment can be generated artificially in a reverberation chamber. This provides a statistically repeatable laboratory-produced environment for characterizing MIMO antennas, by measuring channel capacities. Such a chamber is shown in Fig. 7 below.

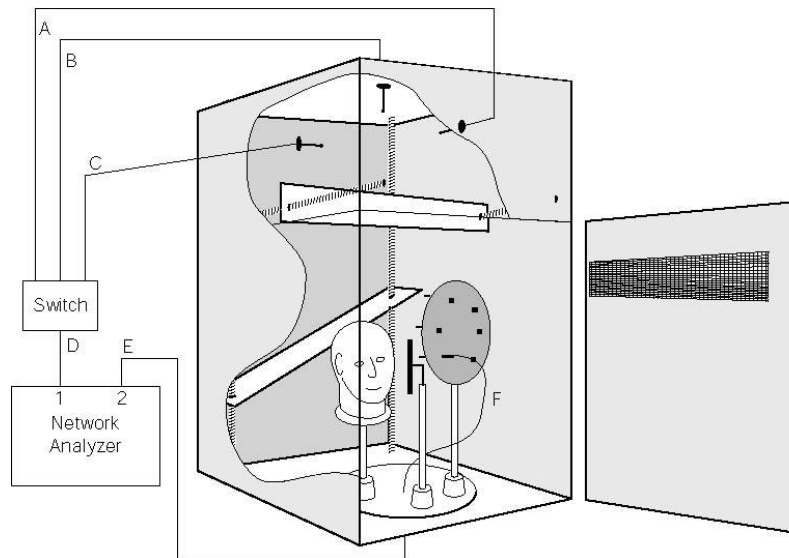


Fig. 7: Schematic drawing of the measurement procedure in reverberation chamber

The procedure for measuring a diversity or MIMO antenna in a reverberation chamber is briefly described as follows. The diversity or MIMO array is located inside the reverberation chamber in such a way that it is more than 0.5 wavelengths from the walls and mechanical stirrers. We also locate a single antenna with known radiation efficiency far enough from the array to avoid significant direct coupling, to produce a reference level (for non-directive antennas a spacing of half to one wavelengths is sufficient). We connect one of the array ports to a source, i.e. a network analyzer, and terminate all the other ports and the reference antenna in 50Ω . We gather S-parameters between the port and the three wall-mounted antennas (used for polarization stirring) for all positions of the platform and the mechanical stirrers and for all frequency points. The measurement procedure is then repeated for every antenna port, also with the unconnected ports terminated in 50Ω , for exactly the same stirrer positions and position of the array inside the chamber. Thus, the field environment is exactly the same when measuring every port. The complex transmission coefficients S_{nm} between the connected port and each of the three fixed wall antennas, as well as the reflection coefficients S_{nn} of each of the wall antennas and S_{nn} of the array port, are stored for every stirrer position and frequency point. Finally, we connect the reference antenna to the network analyzer and perform the same measurements as for the array.

We also normalize the corrected S_{nm} samples to the reference level corresponding to 100% radiation efficiency. This is obtained from the corrected S_{nm} samples measured for the reference antenna, and its known radiation efficiency. We refer briefly to these corrected and normalized samples of S_{nm} as the normalized S_{nm} values. The normalized S_{nm} values represent estimates of the channel matrix \mathbf{H} of multipath communication channels set up between the wall antennas and the MIMO array inside the chamber. Therefore, from the measured S-parameters the instantaneous maximum capacity in each stirrer position can be obtained by using Shannon's formula for capacity:

$$C_{M \times N - \text{MIMO}} = \log_2 \left(\det \left(\mathbf{I}_M + \frac{\text{SNR}}{M} \mathbf{H} \mathbf{H}^* \right) \right)$$

where $M = 3$ is the number of wall-mounted antennas and $N = 4$ the number of ports on the array in our case..



Fig. 8: Photograph of the measurement setup for the reference antenna (left) and the compact array (right).

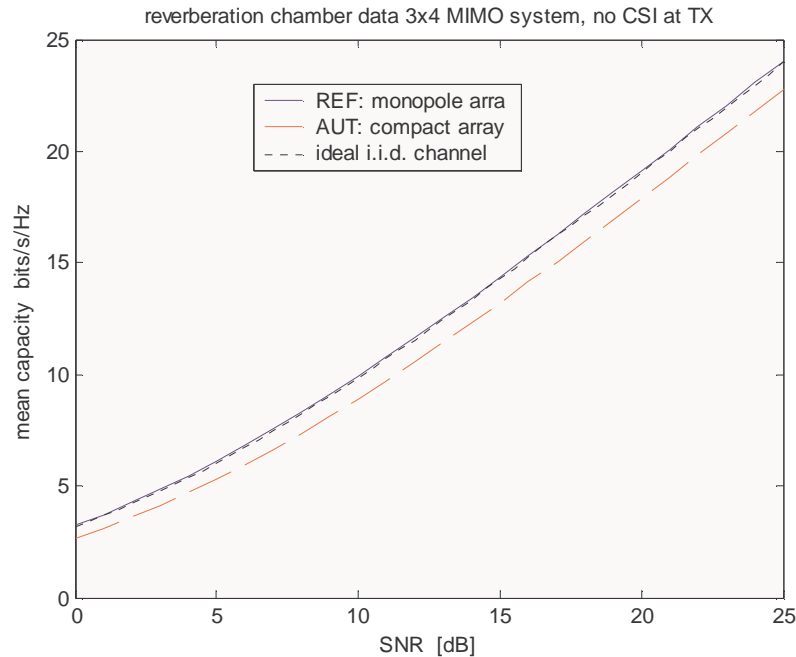


Fig. 9 . Simulated capacity based on reverberation chamber measurement data.

Thus, the reverberation chamber creates a quasi-isotropic field so that a 3 x 4 MIMO system may be tested. The simulated capacity is shown in Fig. 9 above. As expected from the low correlation calculated in the previous section, the capacity curves basically differ as the signal strength varies. We have

- 1 bit/s/Hz difference, or equivalently ~ 1.2 dB, at 10 dB SNR
- 1.2 bits/s/Hz difference at SNR = 25 dB

Again, we find that the primary difference between the arrays may be due to a different as a radiation efficiency.

3.3 Channel measurements at KTH

The baseline for our comparison of different antenna array evaluation methods is a direct channel measurement. These were done using the MIMO test-bed of KTH [10][11] on the 3rd, 4th, and 5th floor of the S3 Department building at KTH. In this report only the data from the 4th floor is used. Fig 10 shows a floor plan with the measurement routes shown in different colour and photographs of the equipment.

The examples that are studied are:

- Environment 1: Hallway-type, with line of sight to the transmitters, route 1 \rightarrow 4), floor 4.
- Environment 2: Hallway-type, without line of sight: measurement 15 (route 4 \rightarrow 5 \rightarrow 8), floor 4.
- Environment 3: Office-type: Conference room, floor 4.

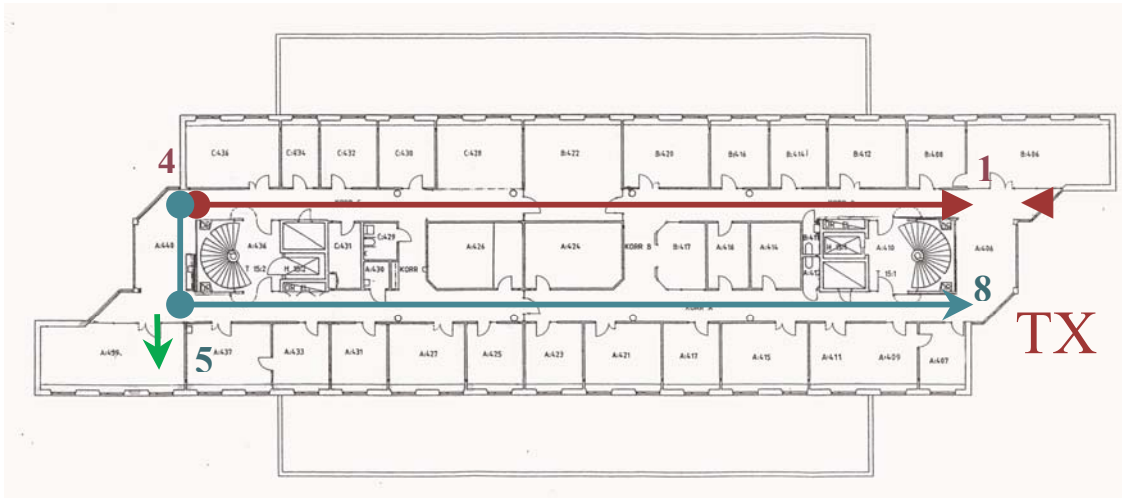


Fig. 10: Plan of the 4th floor of the S3 department at KTH showing the routes 1 (red), 2 (blue), and 3 (green) and photographs of the measurement equipment under calibration (bottom left) and test (bottom right).

For all the cases, several parameters are analysed:

- “power”: it refers to the power of the \mathbf{H} matrix, computed as the square of the Frobenius norm:

$$Pow(\mathbf{H}) = \|\mathbf{H}\|_{Frob} = \sum diag(\mathbf{H}^* \cdot \mathbf{H})$$

where $(\cdot)^*$ represents the complex conjugate. This parameter may help us to see how much power is received by each antenna array (the reference array and the compact array or antenna under test, AUT), and will be used to normalized the H matrix in order to get the capacity for each case.

- Capacity: the capacity is computed assuming no channel state information (CSI) at the transmitter

and perfect channel knowledge at the transmitter. Different normalizations are also considered. The obtained capacities for different cases are compared by means of c.d.f. curves.

- Singular value decomposition of matrix \mathbf{H} and eigenvalue decomposition of matrix $\mathbf{R} = \mathbf{H}^H \mathbf{H}$, where $(\cdot)^H$ represents the complex conjugate transpose. In order to properly evaluate the dispersion of the singular- (γ) and eigenvalues (λ), the ratio of their geometric and arithmetic mean is computed as:

$$\Gamma(n) = \frac{m_{\gamma,g}(n)}{m_{\gamma,a}(n)} = \frac{\left(\prod_{k=1}^K \gamma_k(n) \right)^{1/K}}{\frac{1}{K} \left(\sum_{k=1}^K \gamma_k(n) \right)}, \quad \Lambda(n) = \frac{m_{\lambda,g}(n)}{m_{\lambda,a}(n)} = \frac{\left(\prod_{k=1}^K \lambda_k(n) \right)^{1/K}}{\frac{1}{K} \left(\sum_{k=1}^K \lambda_k(n) \right)}$$

These ratios are a power-invariant measure of the dispersion of the singular and eigen values, respectively, and may help us to understand how similar or different they are. Note that $0 \leq \Gamma \leq 1$ and $0 \leq \Lambda \leq 1$. In the extreme cases, the minimum value is obtained when the parameters are very different, and the maximum when all of them are equal. In our case, the last option would give the ideal K parallel AWGN channels.

3.3.1 Example 1: Hallway LOS, 4th floor, route 1→4¹

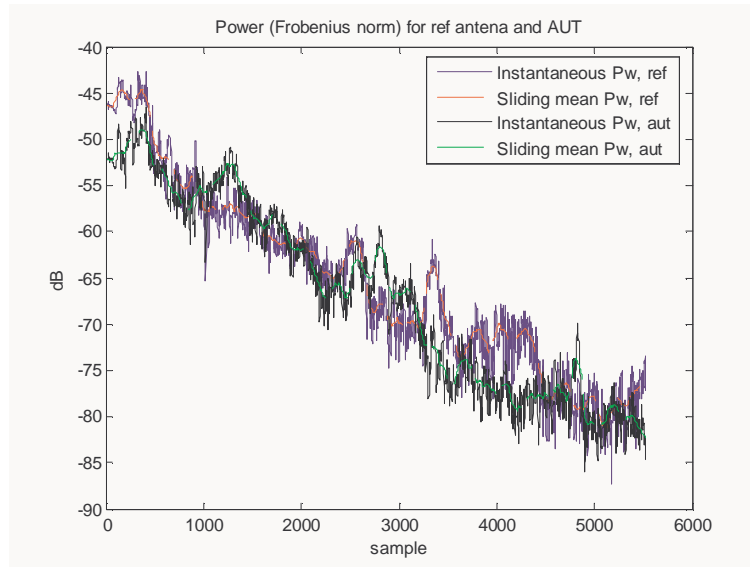


Fig. 11: Instantaneous power and mean sliding power

The “power” or matrix norm is represented as instantaneous values and as a mean value computed with a sliding window of 100 samples. We can notice that the power is higher in most of the cases for the reference array than for the AUT.

The capacity is computed with a normalized \mathbf{H} matrix. The \mathbf{H} matrix is normalized with the instantaneous norm and with the mean sliding norm. The most obvious way of normalizing would be to do it with respect to the reference antenna. However, since the AUT seems to receive less power than the reference antenna, that would make the actual SNR used to compute the capacity be smaller in the case of the AUT than for the reference antenna. On the other hand, if the aim is to compare two antennas performance, the normalization

¹ Measurement file used: Hmatrices\NewHTues_26Oct\H-19-16_09_28.mat'

should be the same for both antennas, since the environment and transmitted signal is the same for both of them. In order to analyse these two cases, results for both normalizations are plotted.

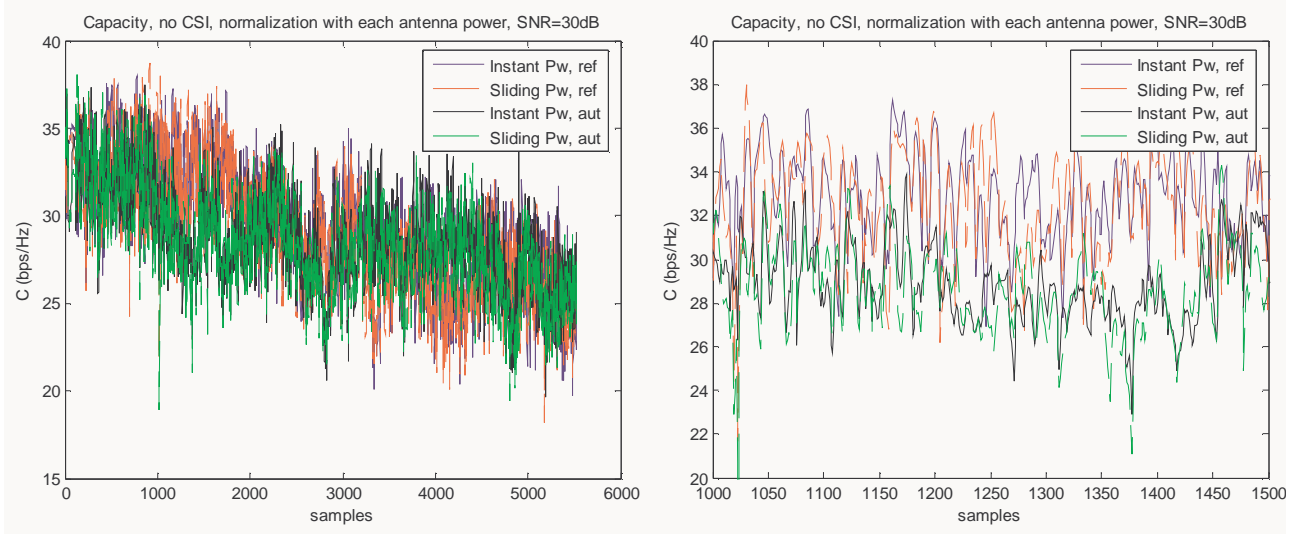


Fig. 12 . Instantaneous capacity for the Hallway LOS, no CSI. The H matrix was normalized with instantaneous power value and with “sliding” mean power. SNR=30 dB. A zoom is included in the figure on the right.

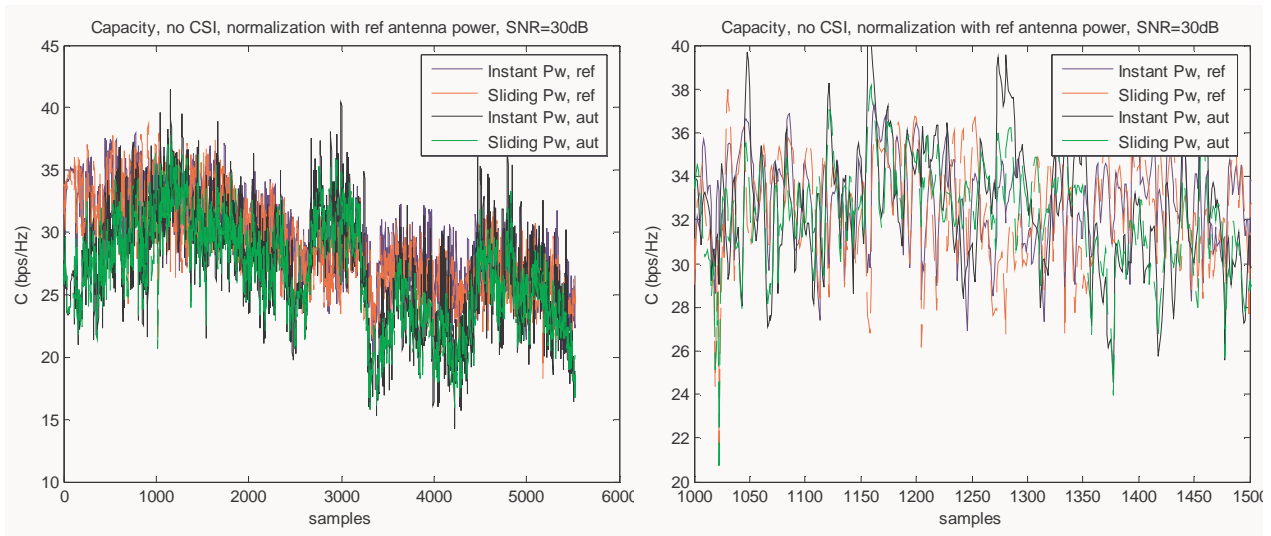


Fig. 13 . Instantaneous capacity for the Hallway LOS, no CSI. Normalization is done with ref_antenna. SNR = 30 dB. A zoom is included in the right figure.

For this time slot (sample 1000 to sample 1500, that is, from $t = 10s$ to $t = 15s$) the norm is higher in the case of the AUT. Thus, when normalizing with the reference antenna norm the AUT capacity increases. Considering this second case (normalization with ref antenna), the capacity is approximately the same for both antennas. However, as we will see in other examples, this is not always the case, since usually the received power is higher for the reference antenna.

The c.d.f. capacity was computed for 2 cases with no CSI: SNR=30 dB (corresponding to the c.d.f. of capacity plotted above) and SNR=10 dB.

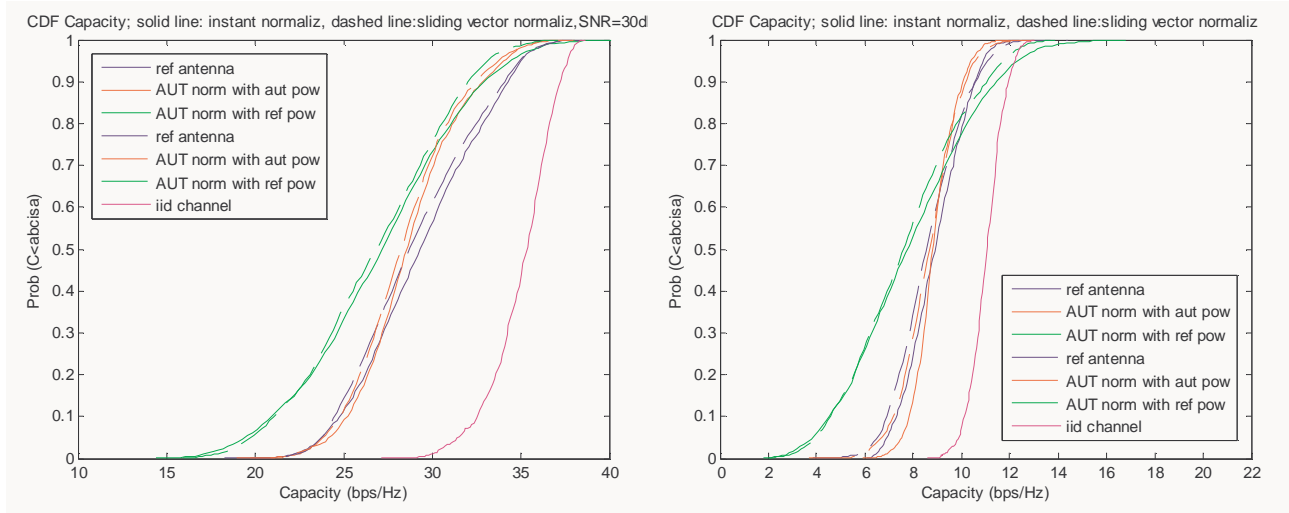


Fig. 14: c.d.f. of the capacity for the Hallway LOS case, no CSI

The pink line [colours are not distinguishable when regular printer is used] is the c.d.f. of the capacity for an i.i.d. channel, which shows the best possible case for no CSI. From the results we observe that:

- Very similar results are obtained for normalization with instantaneous power and sliding vector.
- The capacity for the AUT is very different if H is normalized with the reference antenna power or the AUT power, as expected. As observed in different examples, the performances is always worse in the case of normalization with reference antenna power, since on average the AUT receives less power.
- Considering the normalization with respect to the reference antenna (which seems to be the most reasonable case), the REF antenna presents a better performance than the AUT. The average capacity is higher for the REF antenna, and the variance is smaller so outage capacity for a 10% is also higher in the case of the REF antenna, for both SNR=10dB and 30dB.

Finally, we have compared the case of perfect CSI and no CSI in Fig.15. Notice that the differences between having or not CSI at transmitter are substantial for low SNR, but not for high SNR (as we will see, this is true in the other cases).

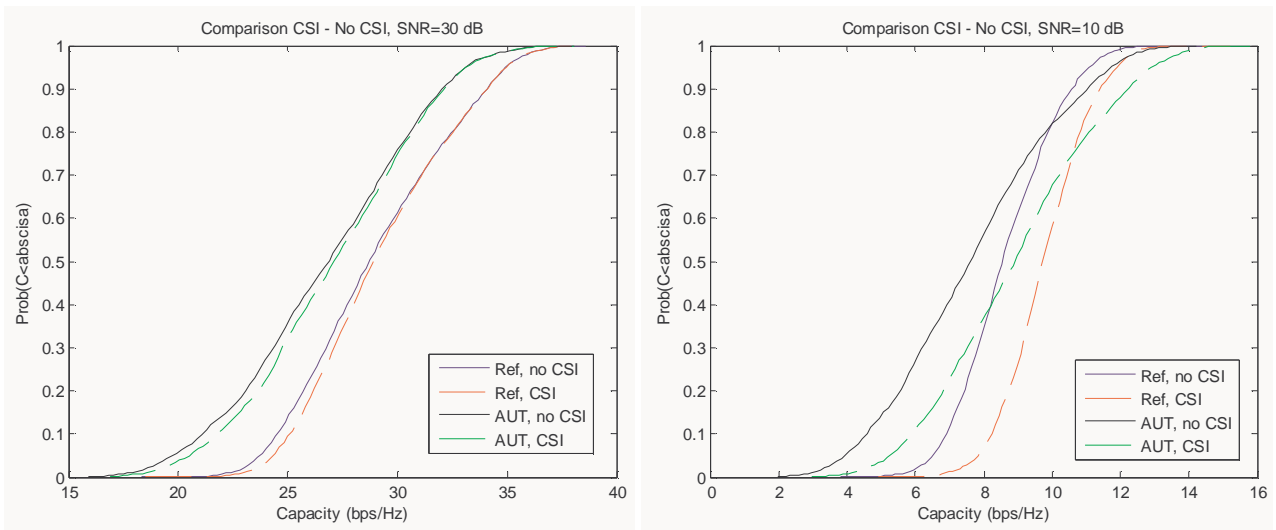


Fig. 15 : Comparing capacity for the Hallway LOS case with/without CSI at TX, for different antennas and SNR.

Singular value decomposition (SVD) and Eigenvalue decomposition (EVD) have been obtained for both antenna settings. Fig. 16. depicts the SVD for the REF antenna and AUT. We can see a sudden decrease of singular normalized values for certain instants ($t=[24\dots26.5]$, $t=[34\dots35]$ and $t=[40\dots43]$ are slots with decreased singular values for the reference antenna, while the reduction is not so evident for the AUT).

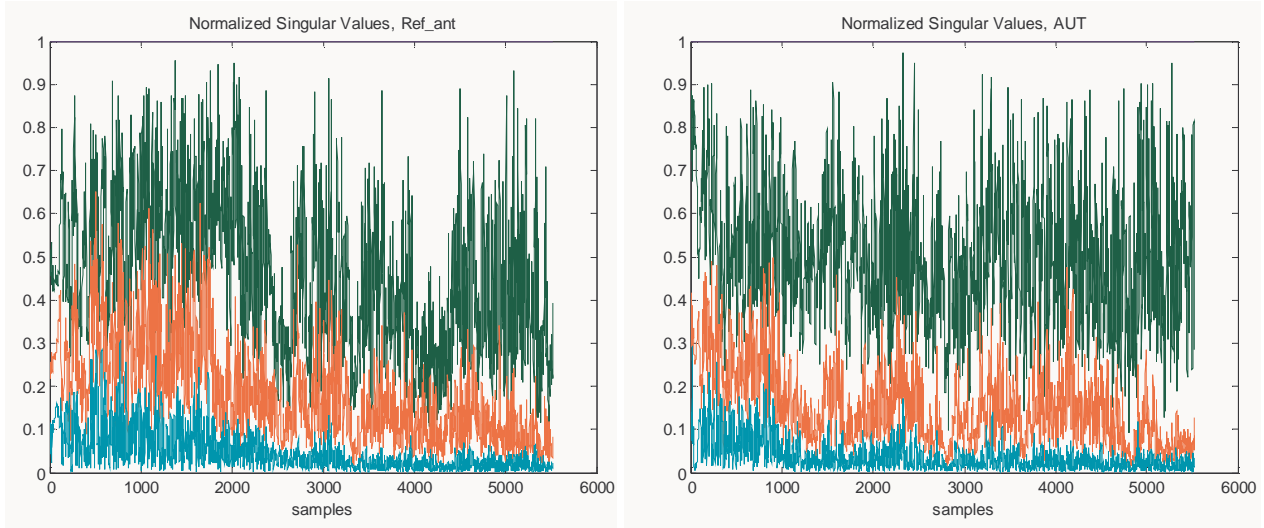


Fig. 16: Comparing singular value decomposition the Hallway LOS case at SNR = 10 dB

The c.d.f. for the dispersion of singular values for both arrays shows that the reference antenna seems to perform slightly better in that case, regarding singular values dispersion (and therefore diversity). As we will see for other examples, that is not the case in other environments and situations. Not a big difference can be observed for this case. For other cases, the differences are more significant (see below).

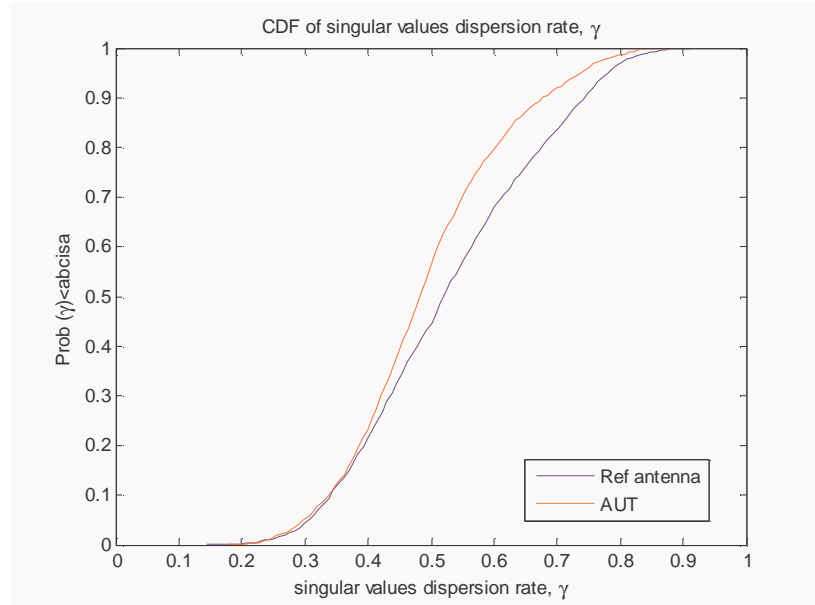


Fig. 17: Singular value dispersion rate for the Hallway LOS case.

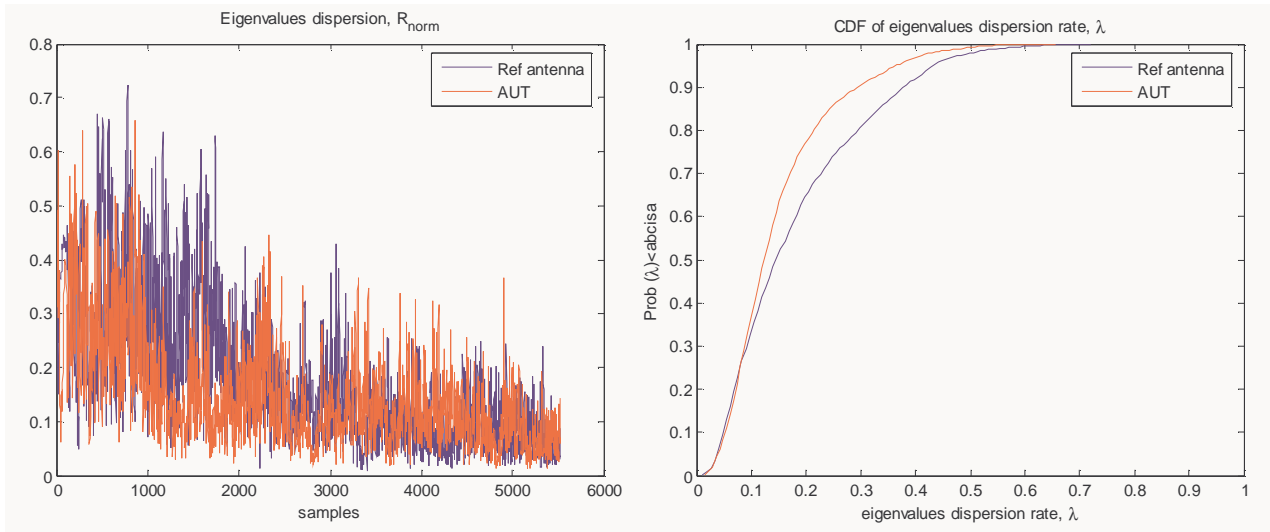


Fig. 18 . Comparing eigenvalue dispersion of $R=H^H H$ for the Hallway LOS case, SNR=10dB.

Similarly, Fig. 18 compares the eigenvalue dispersion of the covariance matrix for both antenna settings. Similar results to the singular value decomposition are observed. Again, a slightly better performance is achieved with the REF antenna for this case. Notice that in this measurement, not much difference in capacity or SVD is seen when the receiver arrives at the crossing between hallways (wp2 or wp3, in $t=22.88$ sec and $t=40.2$ sec respectively).

3.3.2 Example 2: Hallway NLOS, 5th floor, route 4→8²

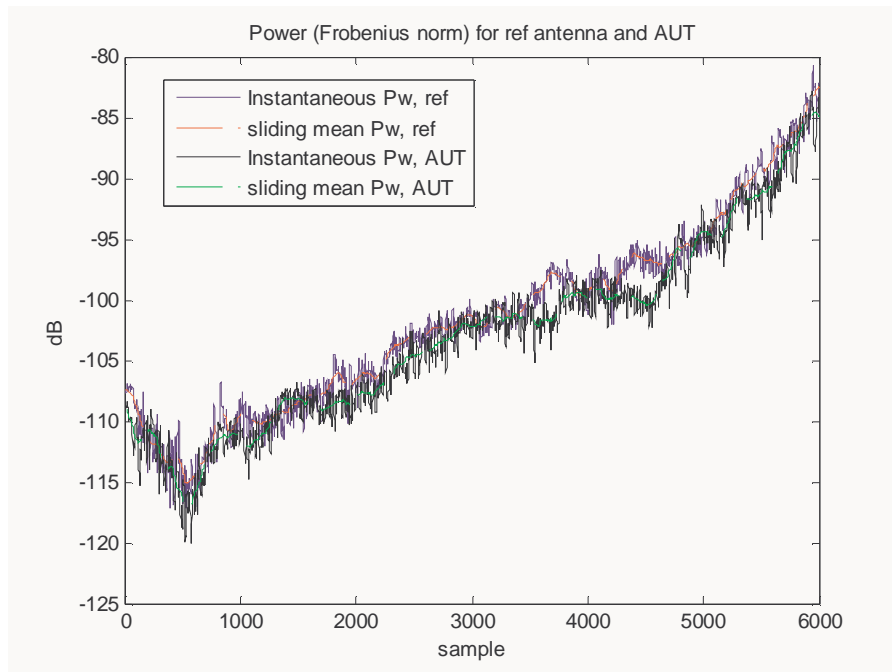


Fig. 19 . Instantaneous power and mean sliding power for the Hallway NLOS case.

² Computed data: Hmatrices\NewHTues_26Oct\H-19-16_51_58.mat'.

In this measurement, where the receiver is moving one floor above the transmitter, the power is quite similar for both antennas. That may indicate that the monopole reference array is able to collect more power in the hallway when there is line of sight with the transmitters, even if the TX antennas were slanted-polarized ones. The hallway in LOS may work as a “guide” for the vertical polarization, while in the case of this measurement (in 5th floor) the “guide effect” is not so clear.

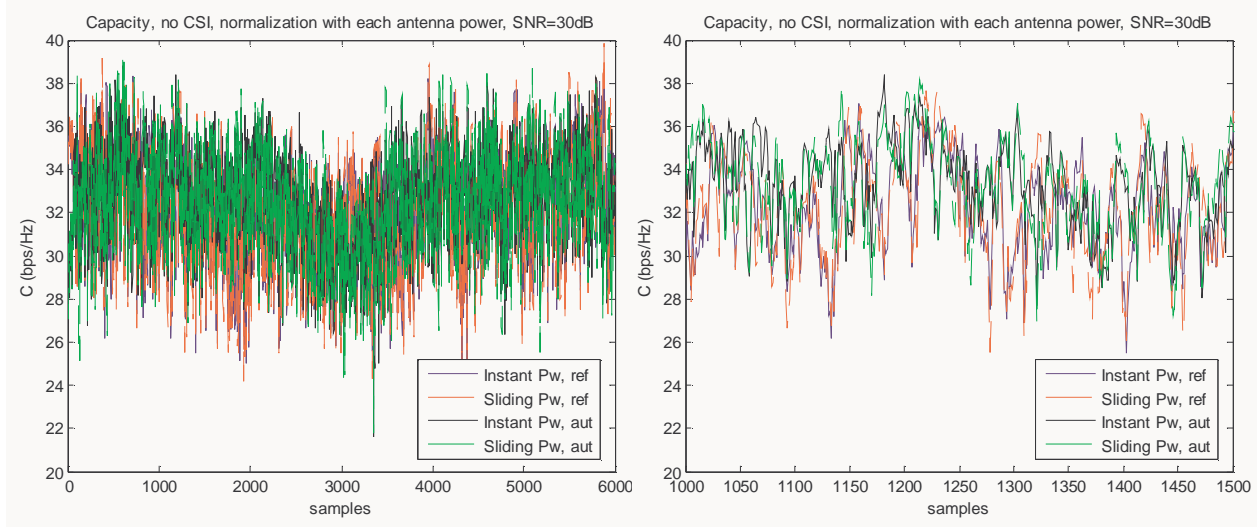


Fig. 20: Instantaneous capacity for the Hallway NLOS case, no CSI. The H matrix was normalized with instantaneous power value and with “sliding” mean power. SNR=30 dB. Each array is normalized with its own power vector. A zoom is included in the figure on the right.

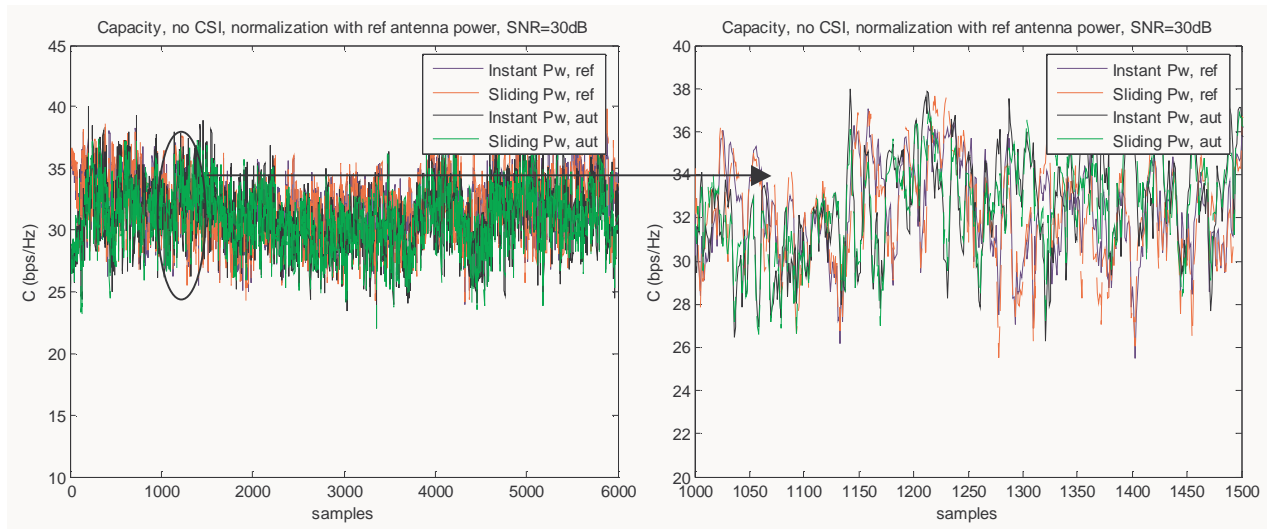


Fig. 21 . Instantaneous capacity for the Hallway NLOS case, no CSI. Normalization is done with ref_antenna. SNR = 30 dB. A zoom is included in the figure.

Since there are not significant differences in the power, there are none in the capacity when comparing with the two normalizing approaches. The c.d.f. of the capacity was computed for two different cases when no CSI is available: SNR=30 dB (corresponding to the CDF of capacity plotted above) and SNR=10 dB.

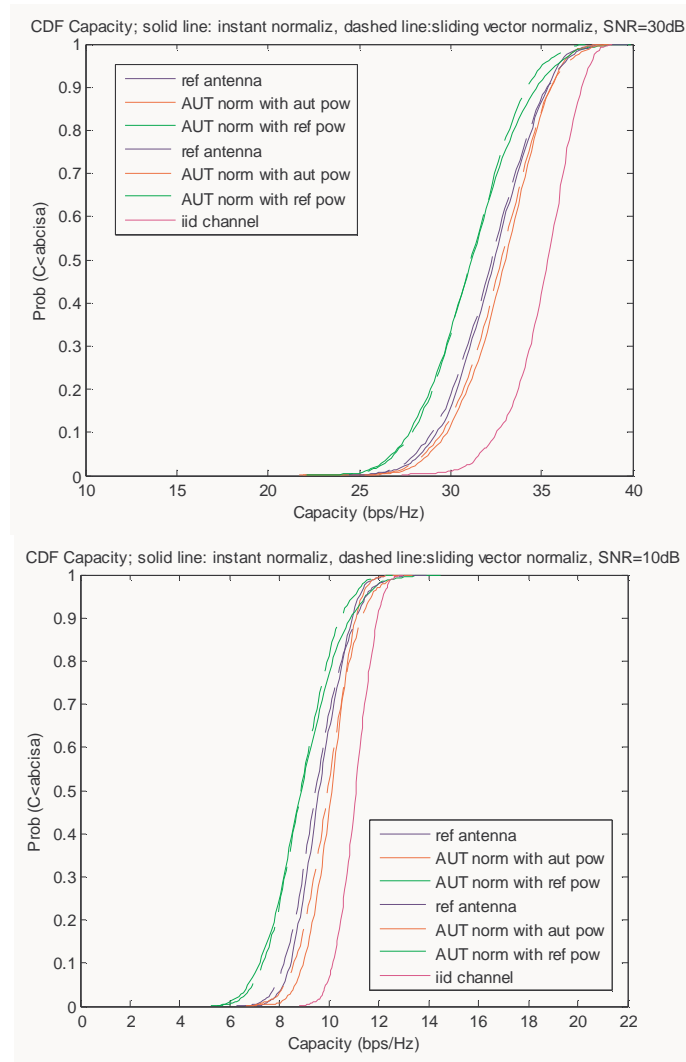


Fig. 22: c.d.f. of the capacity for the Hallway NLOS case , no CSI

It can be observed that the differences between the reference antenna and the AUT are much smaller for this case than for the LOS case. Nevertheless, the AUT performs worse than the reference antenna when the normalization is done with the reference antenna power. Note also that the average capacity is higher in this case (NLOS) than in the LOS case, as expected.

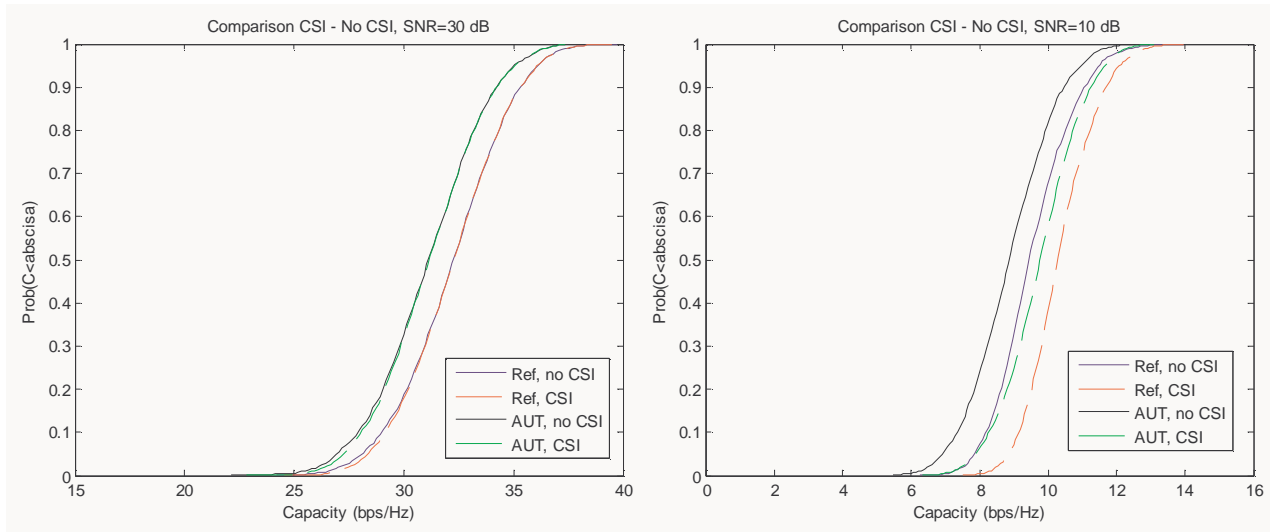


Fig. 23: Comparing capacity for the Hallway NLOS case with/without CSI at TX, for different antennas and SNR

Singular value decomposition (SVD) and Eigenvalue decomposition (EVD) have been obtained for both antenna settings in this scenario, with results depicted in Fig. 24. In this case, the AUT seems to achieve a slightly higher dispersion in singular values than the reference antenna. Note also that the dispersion is larger in this case than in the LOS case, which leads to a higher capacity for both antenna arrays.

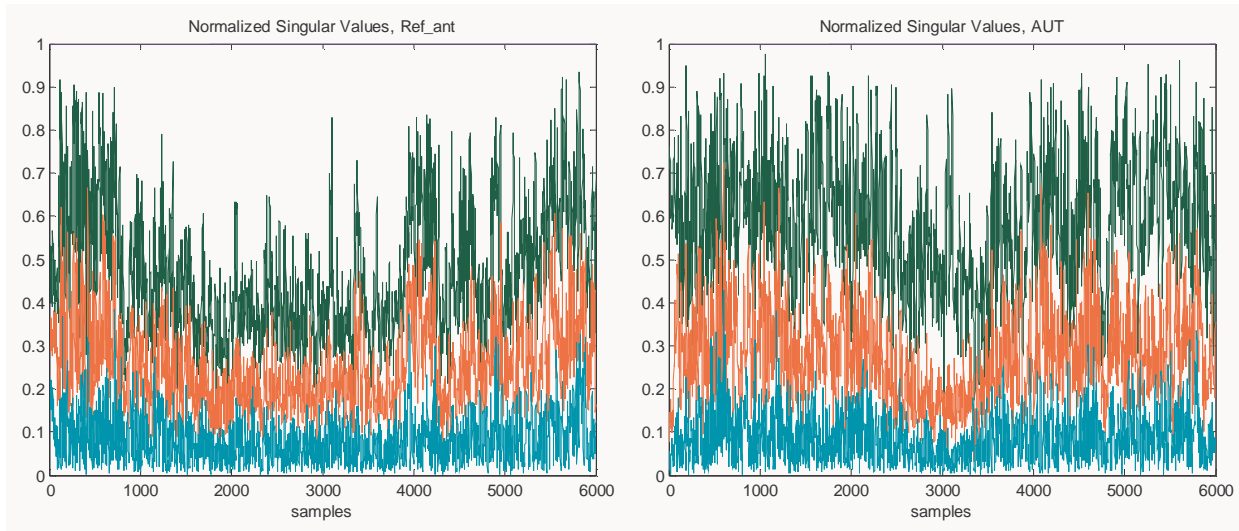


Fig. 24: Comparing singular value decomposition for the Hallway NLOS case at SNR=10dB.

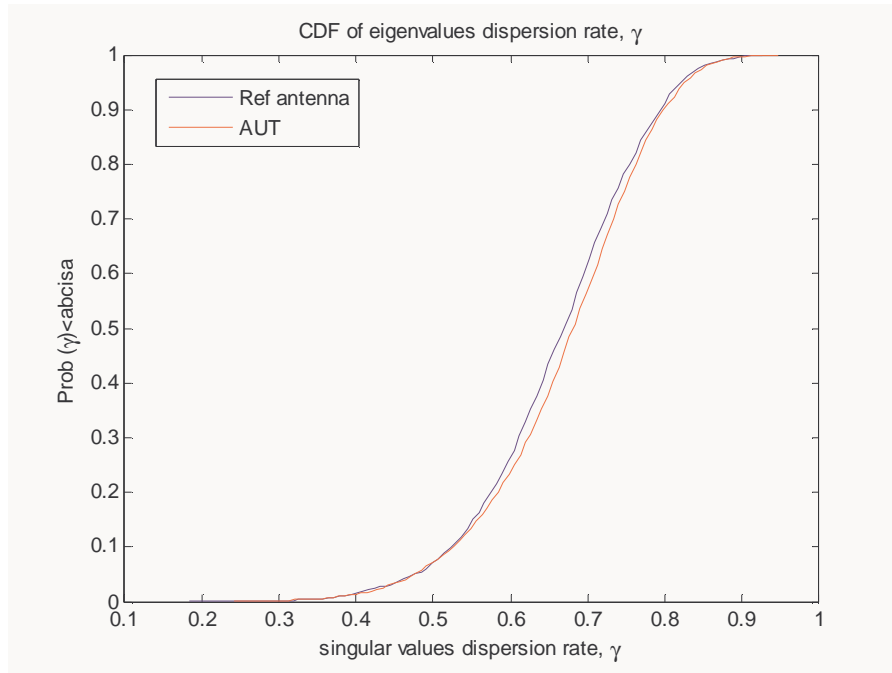


Fig. 25: Singular value dispersion rate for the Hallway NLOS case.

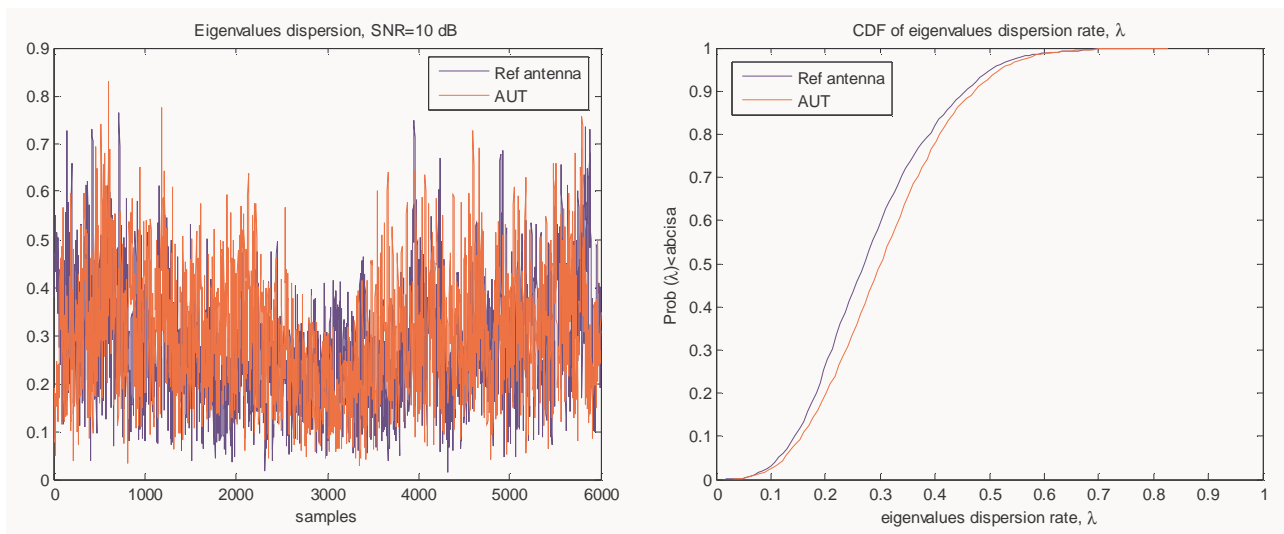


Fig. 26 . Comparing eigenvalue dispersion of $R=H^H H$ for the Hallway NLOS case, SNR=10dB.

3.3.3 Example 3: Office-like environment, 4th floor, Conference room³

The last measured scenario considers an office type environment which is located out of LOS at the far end of the 4th floor seen from the transmitter. Fig. 27 shows the received power. A large difference can be observed in this case: the AUT has an \mathbf{H} matrix with much smaller norm for most of the positions. Also notice that the variance is large in the fast fading.

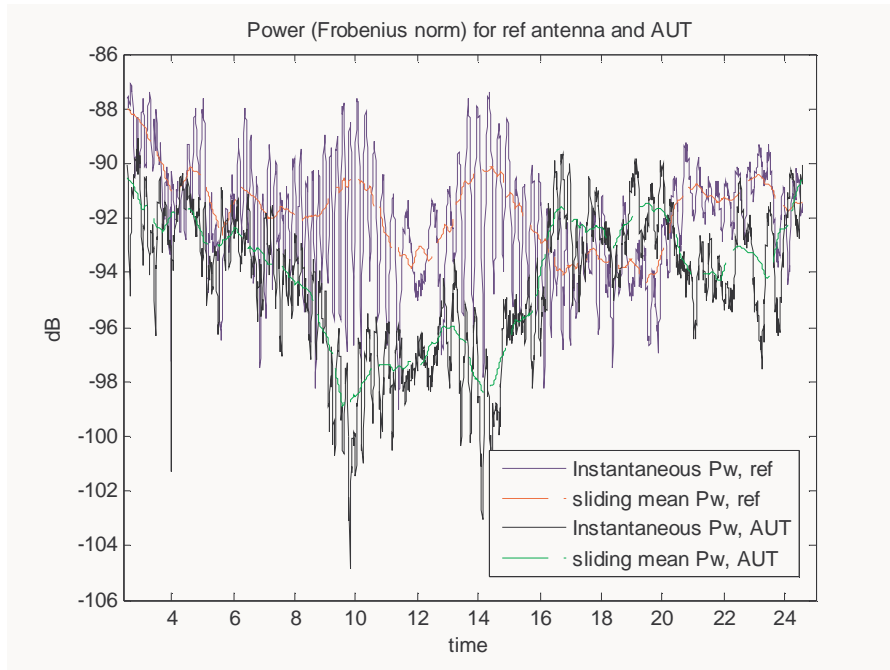


Fig. 27: Instantaneous power and mean sliding power for the Office case.

³ Computed data: Hmatrices\NewHTues_26Oct\H-19-16_33_45.mat'.

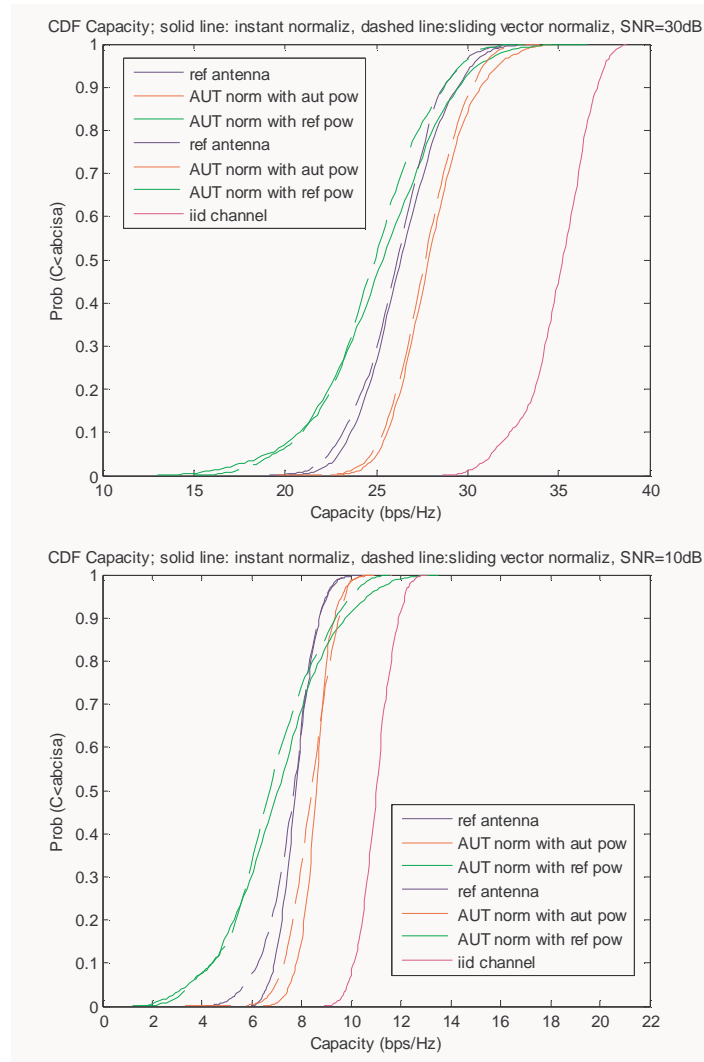


Fig. 28: Instantaneous capacity for the Office case, no CSI. The H matrix was normalized with instantaneous power value and with “sliding” mean power. SNR=30 dB. Each array is normalized with its own power vector. A zoom is included in the figure on the right.

As seen in Fig. 28, the achieved capacity for the AUT when normalizing with respect to its own power is higher than the one obtained with the reference antenna. That means that the obtained diversity is bigger with the AUT than with the reference antenna (this will be validated with the evaluation of SVD and EVD dispersion). However, since the average power that is available with the AUT is smaller than the one received with the reference antenna, the achieved capacity when both measures are normalized with respect to the REF antenna power is higher for the REF array.

Notice that the average capacity is smaller in this case (office-like environment) than in the other two (hallway-like environment) which indicates that we have a “keyhole effect”. As before, we compare the capacity for CIS and no CSI and we again see greater differences for lower SNR.

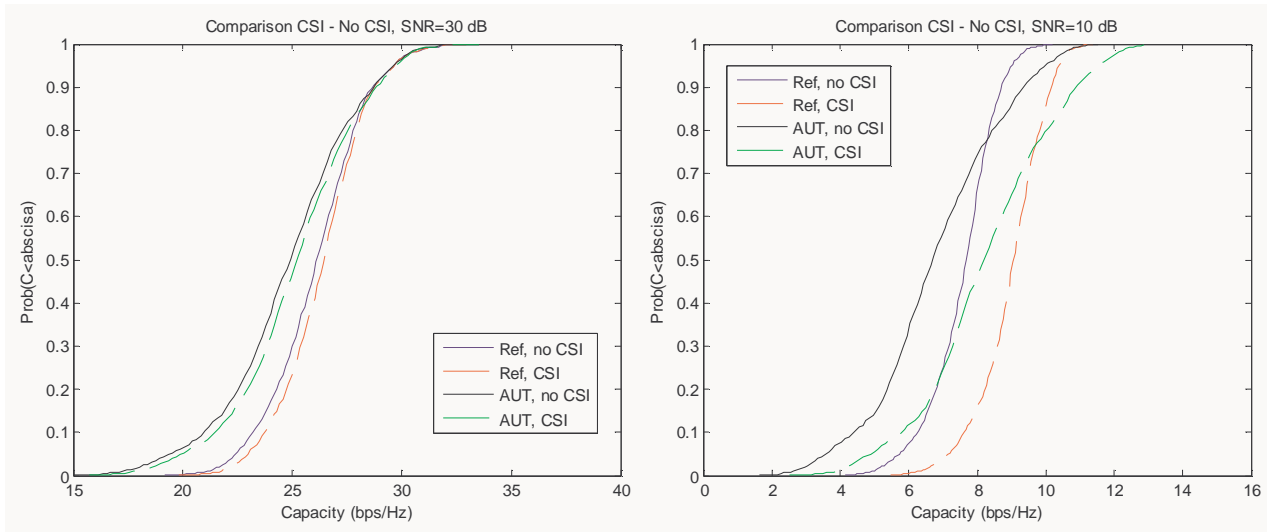


Fig. 29: Comparing capacity for the office case with/without CSI at TX for different antennas and SNR

The singular value decomposition (SVD) and eigenvalue decomposition (EVD) results for this third scenario are shown in Fig. 30, Fig. 31 and Fig. 32.

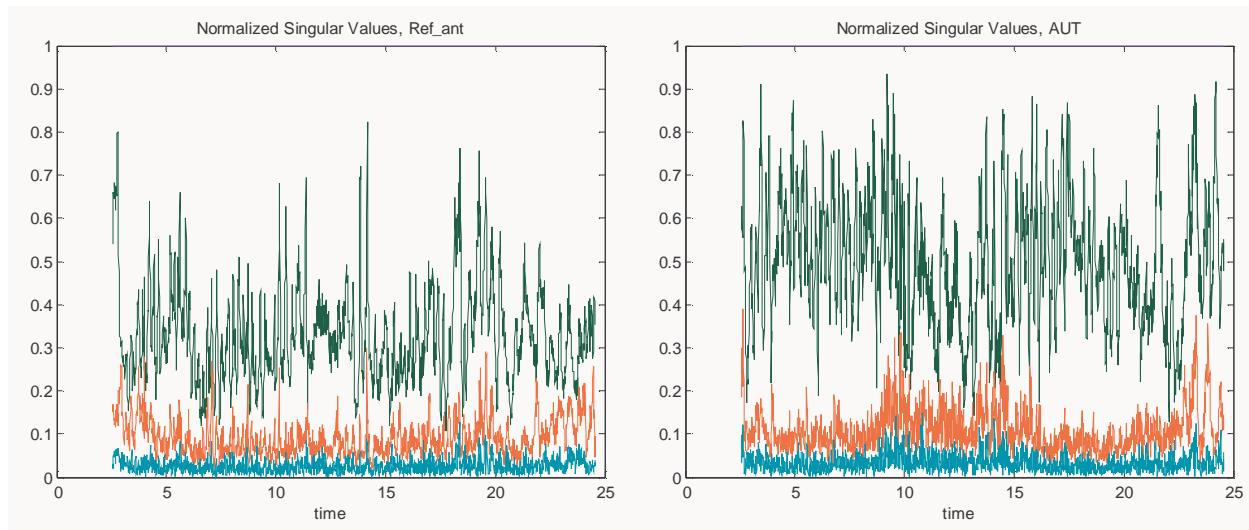


Fig. 30: Comparing singular value decomposition at SNR = 10 dB for the Office case.

For this case, the SVD shows much higher normalized singular values for the AUT, especially the second singular value (green). However, when plotting the singular values without normalizing to the first one, it can be seen that they are smaller for the AUT, which is reasonable considering that the H norm is much smaller in the AUT case. Finally, we study the dispersion rates in Figs. 31-32. Quite a big difference between the 2 antennas is observed. For both the SVD and the EVD dispersion, the value is the smallest of the 3 analysed examples, which makes sense with the small achieved capacity.

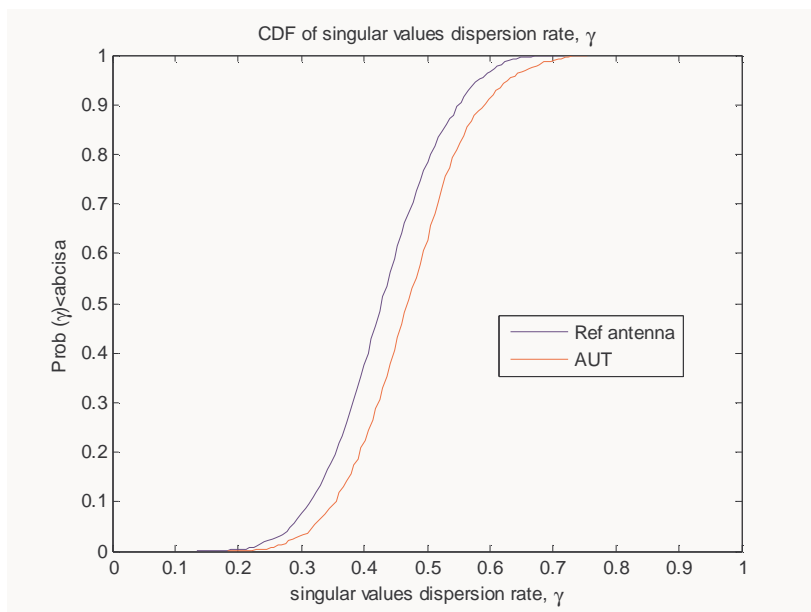


Fig. 31: Singular value dispersion rate for the Office case.

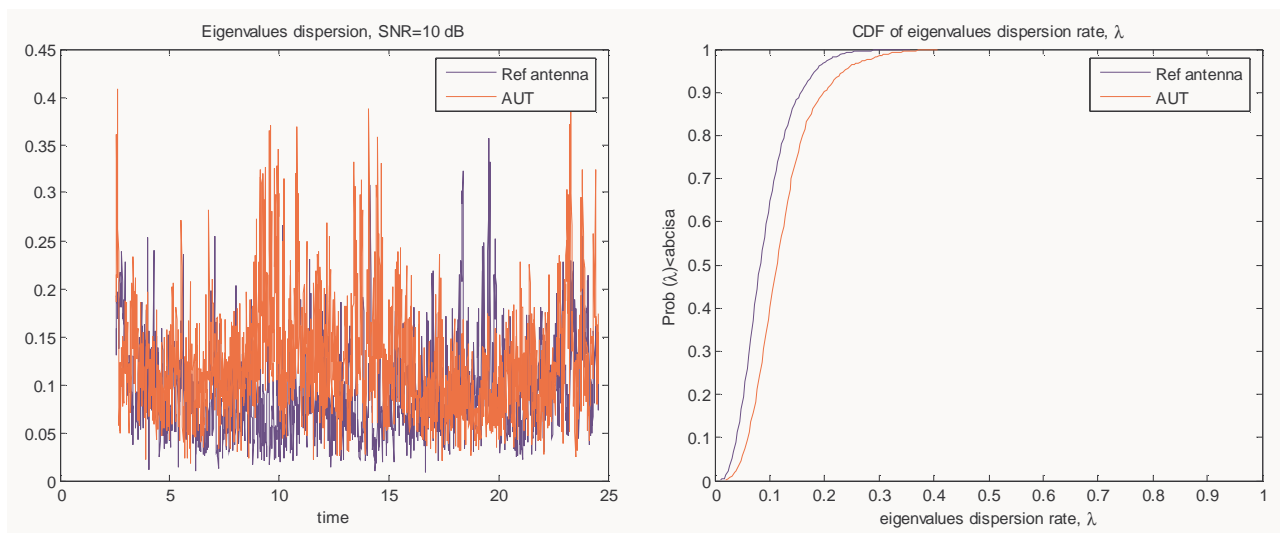


Fig. 32: Comparing eigenvalue dispersion of $R=H^H H$ for the Office case, SNR=10dB.

4 The effect of the human body

After receiving from KTH the CST files with the model of the compact antenna array (on a PDA), we have developed (using CST) a number of models to investigate the influence of the user's hand and the user's body on antenna (AUT) characteristics. A number of cases are possible:

- A0 Reference
- A1 AUT free space
- A2 AUT in hand (“multimedia viewing position”)
- A3 AUT on body (“pocket position”)

Following the first draft proposal distributed after the meeting in Athens (Rev.0.1 Draft A, 10/Feb/2005), we have considered the scenarios A1 (AUT in free space), A2 (AUT in hand, “multimedia viewing position”) and A3 (AUT on body, “pocket position”).

4.1 AUT in HAND

Two simulation test cases for the A2 scenario (A2a and A2b) with different hand models have been proposed and simulate.

- one with homogeneous hand (A2a) and
- the other with 2-layer hand model (A2b).

In the Fig. 33 and Fig. 34, the two models are presented together with the corresponding dielectric properties of the hand materials (at 1800 MHz) [1]. The number and the position of the array elements are also presented on the PDA.

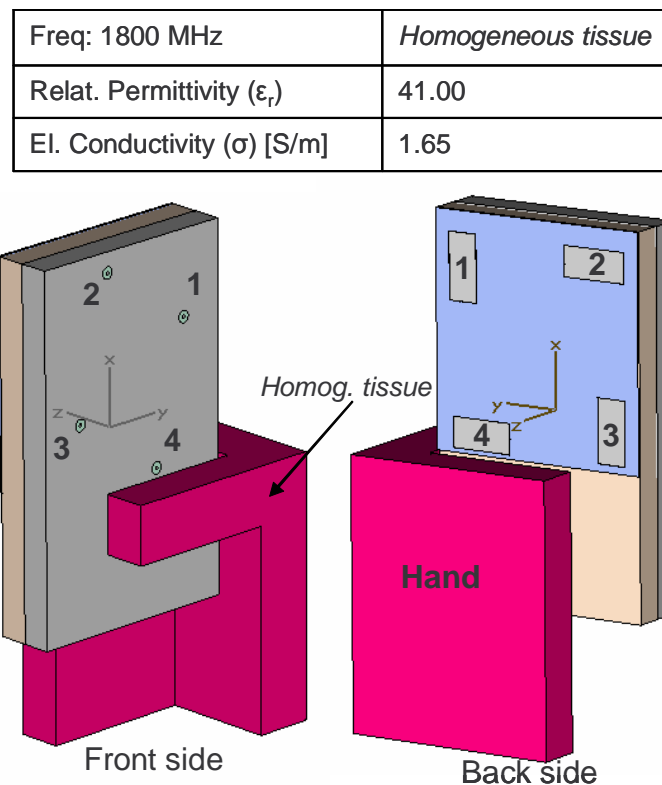


Fig. 33. Homogeneous hand model (test case A2a)

Freq: 1800 MHz	<i>Bone</i>	<i>Muscle</i>
Relat. Permittivity (ϵ_r)	15.56	54.44
El. Conductivity (σ) [S/m]	0.432	1.389

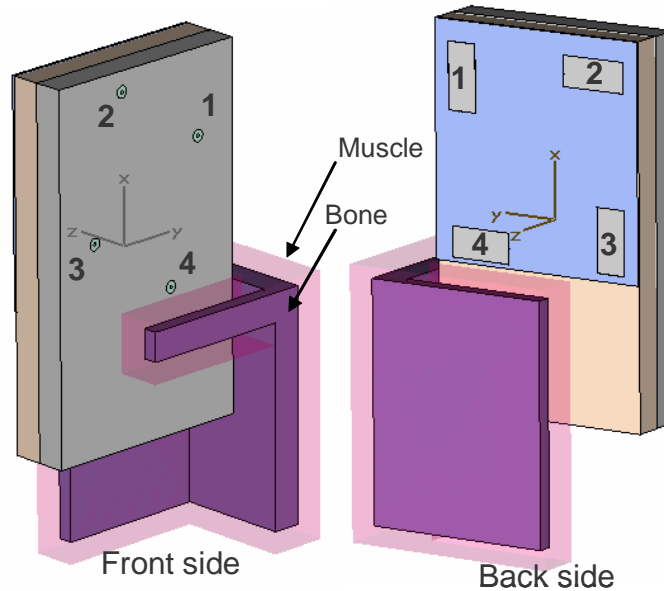


Fig. 34. 2-layer (bone and muscles) hand model (test case A2b)

The output of the simulations includes:

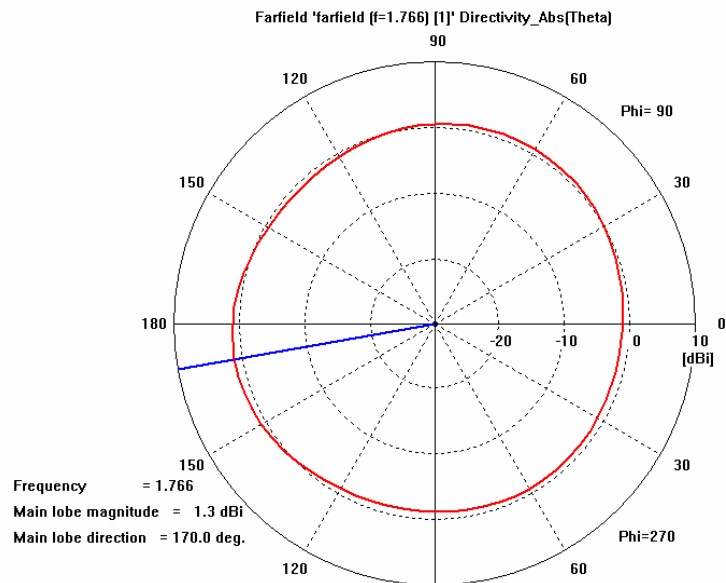
- The **radiation diagrams** (directivity) for each array element (1,2,3,4) and each one of the three test cases (A1, A2a and A2b),
- the **reflection coefficients** (S_{ii}) for each array element and each one of the three cases and
- the **mutual impedance matrix** between the array elements for each one of the three cases.

In the next figures there is a graphical presentation of the above simulation results.

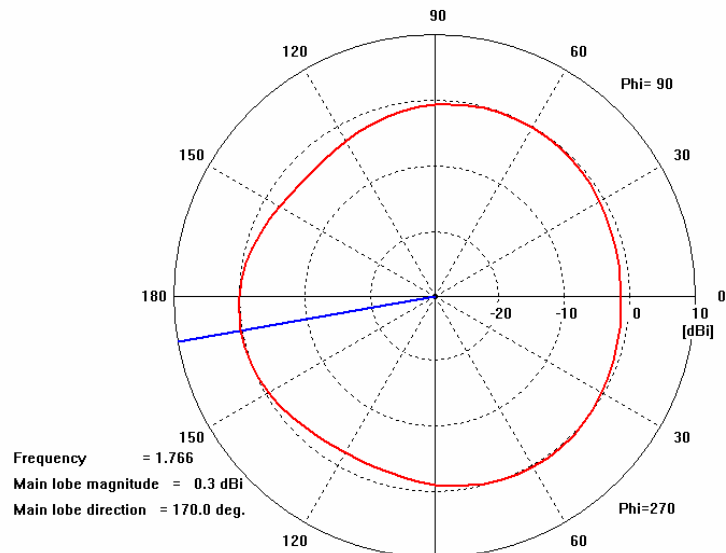
The presented radiation diagrams are referred to the z-y plane (horizontal plane) ($\phi=90 / 270$ degree and $\theta=0$ to 180 degrees). The simulation results for every antenna element are derived considering that the other three elements are terminated with 50 ohms load.

Fig. 35. Element 1 radiation diagrams

(A1) in free space



(A2a) with a homogeneous hand model



(A2b) with 2-layer hand model

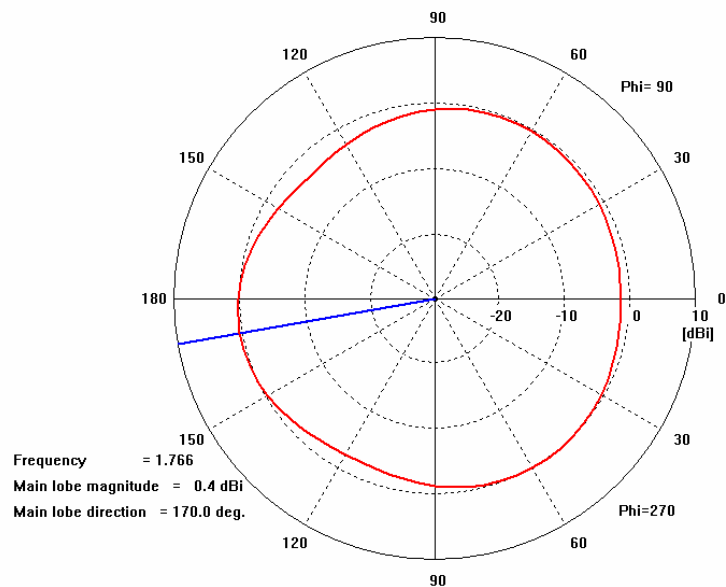
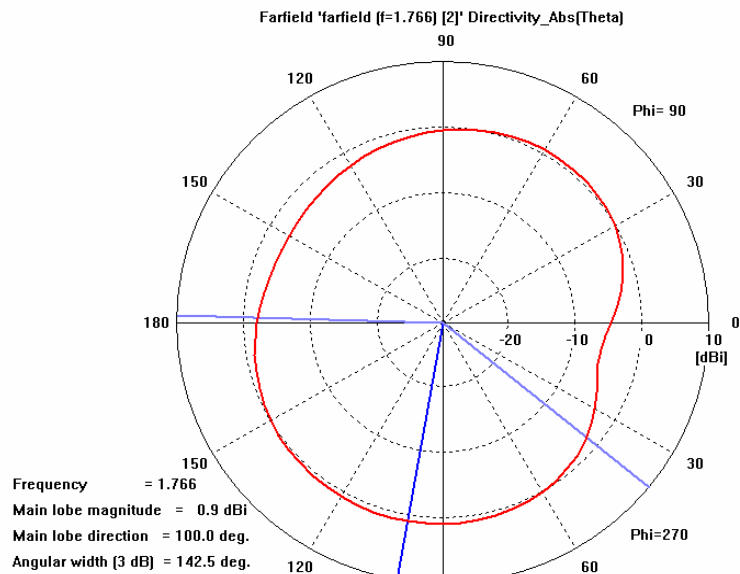
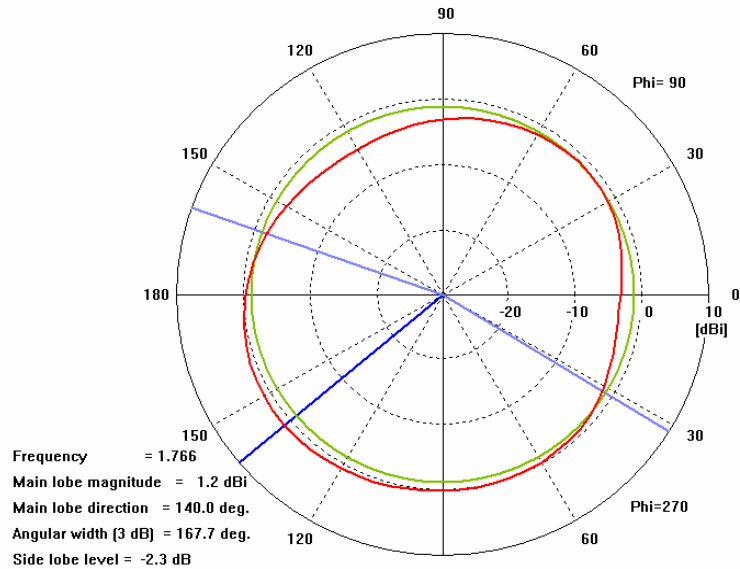


Fig. 36. Element 2 radiation diagrams

(A1) in free space



(A2a) with a homogeneous hand model



(A2b) with 2-layer hand model

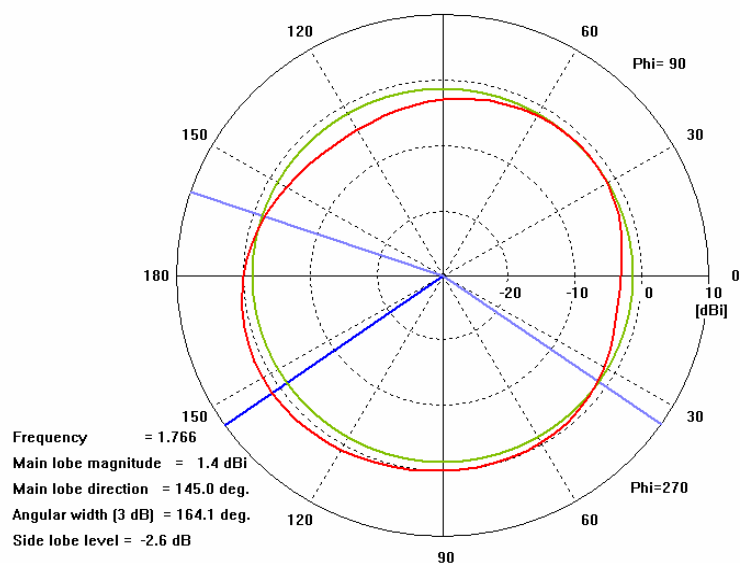
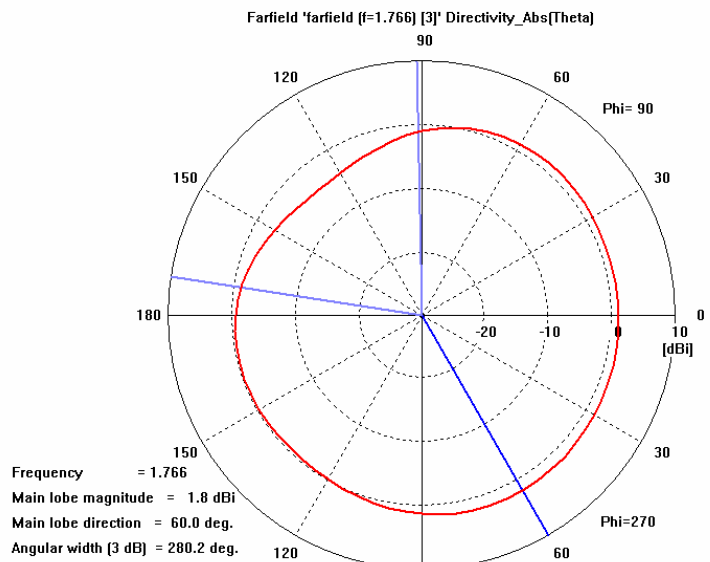


Fig. 37. Element 3 radiation diagrams

(A1) in free space

(A2a) with a homogeneous hand model



(A2b) with 2-layer hand model

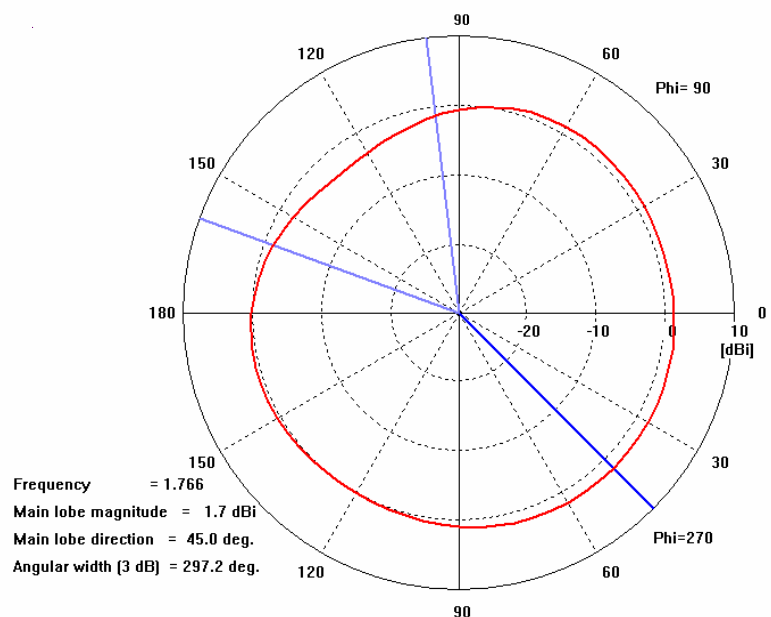
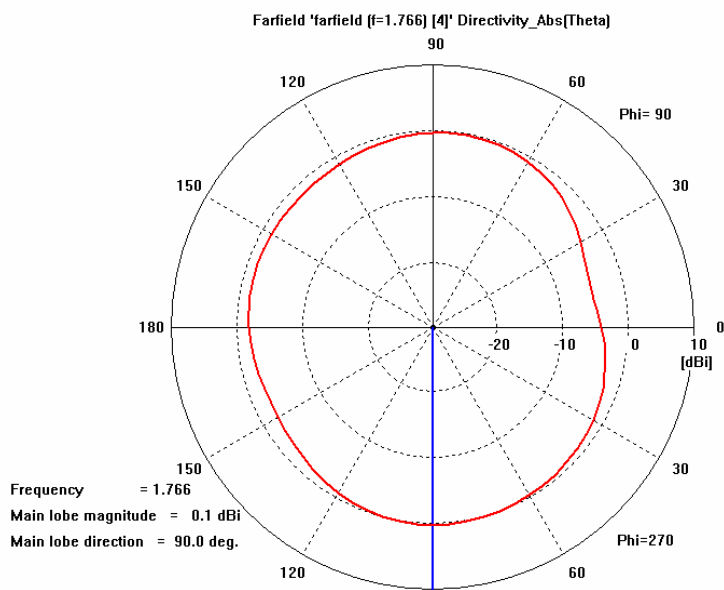
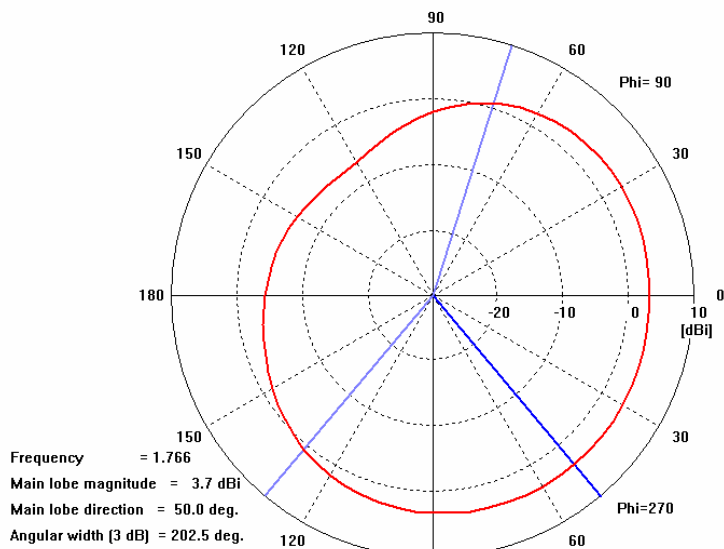


Fig. 38. Element 4 radiation diagrams

(A1) in free space



(A2a) with a homogeneous hand model



(A2b) with 2-layer hand model

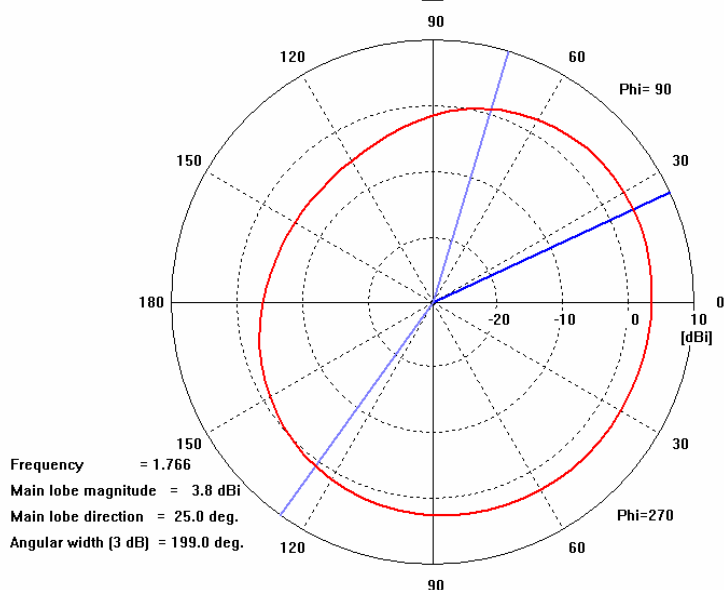
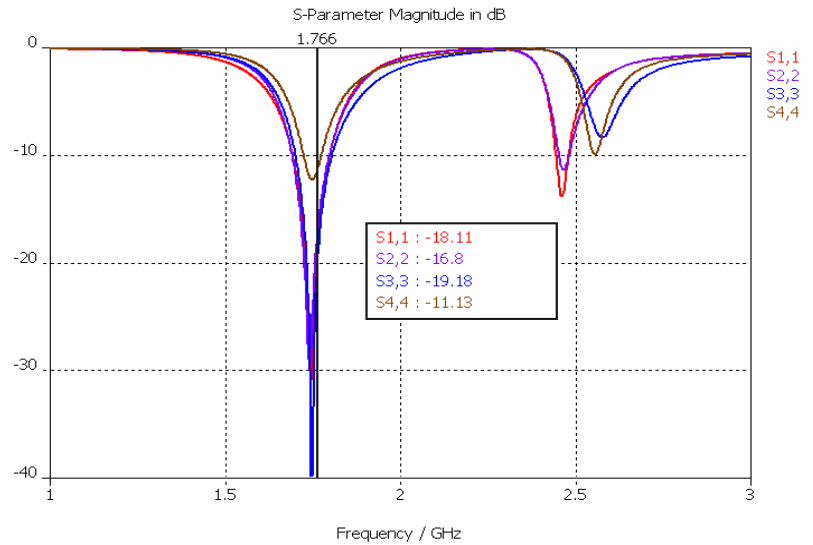
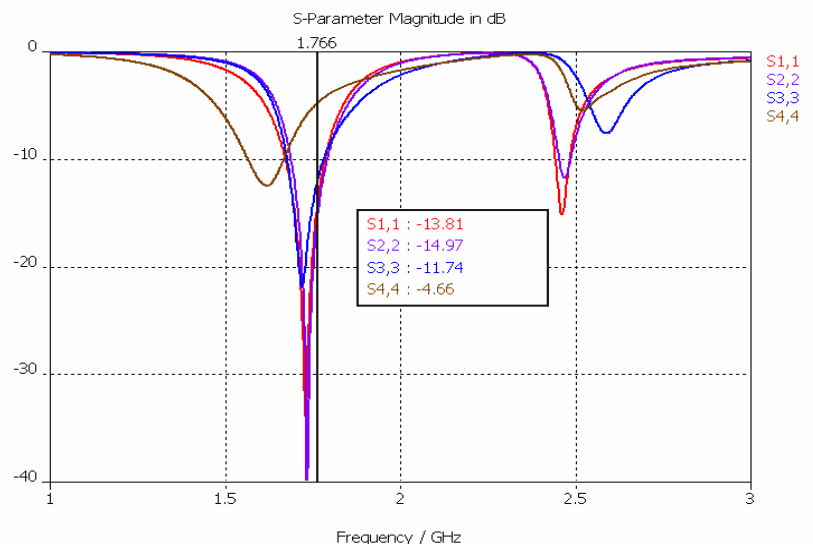


Fig. 39. Reflection coefficients (S_{ii})

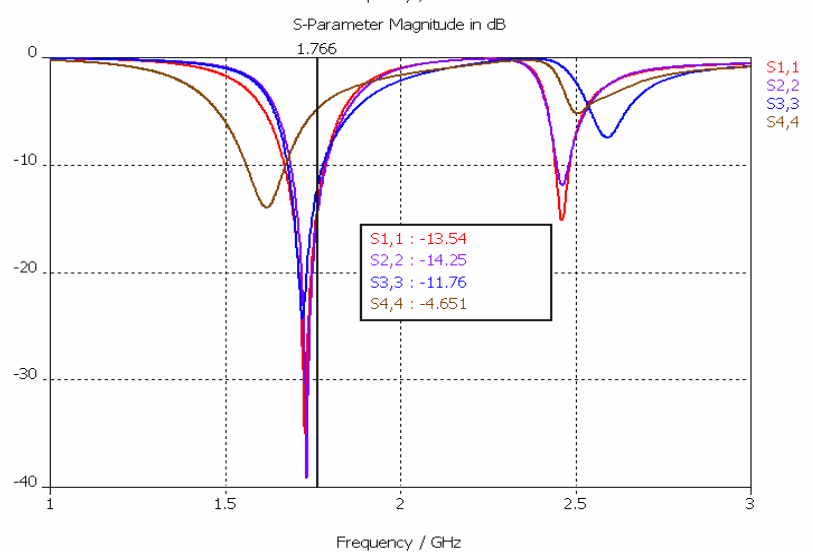
(A1) in free space



(A2a) with a homogeneous hand model



(A2b) with 2-layer hand model



The **mutual impedance matrices** for the corresponding three test cases are given below:

$$(A1) \quad Z_{matrix} = \begin{bmatrix} 44.1 + j4.483 & 9.072 - j16.47 & 4.494 - j4.051 & 15.64 - j8.977 \\ 9.076 - j16.44 & 41.1 + j0.091 & 21.1 - j23.17 & 3.077 - j13.17 \\ 4.5 - j4.046 & 21.1 - j23.17 & 48.45 + j1.53 & 20.78 + j2.102 \\ 15.64 - j8.982 & 3.083 - j13.17 & 20.8 + j2.115 & 33.91 + j2.94 \end{bmatrix}$$

$$(A2a) \quad Z_{matrix} = \begin{bmatrix} 38.69 + j12.35 & 9.311 - j13.37 & 3.175 - j0.5622 & 10.52 - j2.042 \\ 9.331 - j13.36 & 42.61 + j2.6 & 26.57 - j20.46 & 7.91 - j7.558 \\ 3.176 - j0.5767 & 26.57 - j20.44 & 58.25 + j13.88 & 26.11 + j5.354 \\ 10.51 - j2.055 & 7.909 - j7.556 & 26.13 + j5.354 & 46.86 + j64.86 \end{bmatrix}$$

$$(A2b) \quad Z_{matrix} = \begin{bmatrix} 38.29 + j13.2 & 9.236 - j13.27 & 2.495 - j0.017 & 8.975 - j1.258 \\ 9.227 - j13.25 & 42.39 + j3.958 & 26.83 - j18.67 & 8.621 - j5.098 \\ 2.488 - j0.029 & 26.82 - j18.64 & 55.36 + j15.13 & 23.24 + j7.195 \\ 8.976 - j1.276 & 8.623 - j5.098 & 23.26 + j7.201 & 43.25 + j63.81 \end{bmatrix}$$

Where:

$$Z_{matrix} = \begin{bmatrix} Z_{11} & Z_{12} & Z_{13} & Z_{14} \\ Z_{21} & Z_{22} & Z_{23} & Z_{24} \\ Z_{31} & Z_{32} & Z_{33} & Z_{34} \\ Z_{41} & Z_{42} & Z_{43} & Z_{44} \end{bmatrix}$$

4.2 AUT on BODY

In order to investigate the influence of the user's body on the characteristics of the AUT in the case of “pocket position” we have adopted a simplified model for human body simulated by a simple dielectric cylinder. The size and dielectric properties of this model are given in the next figure. The idea of using this model is based on the “salty man” model used in EMC test measurements [2]. The advantage of this model, in addition to its simplicity, is that it can be easily implemented to perform reproducible measurements in real environment.

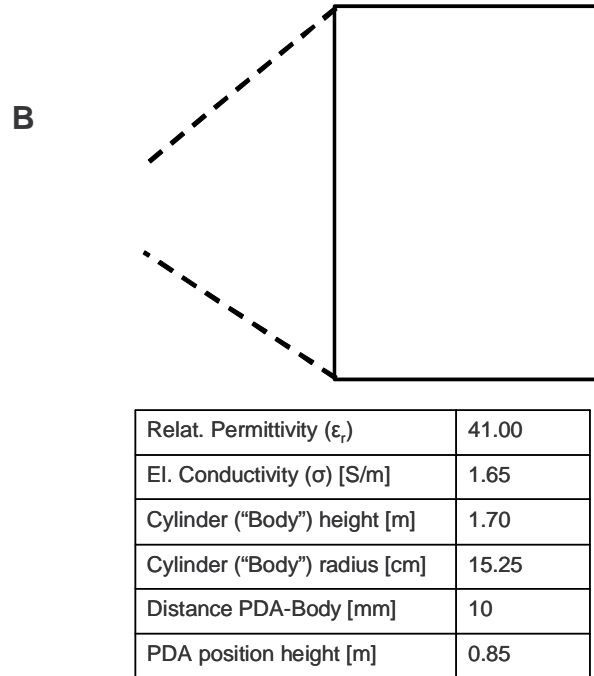


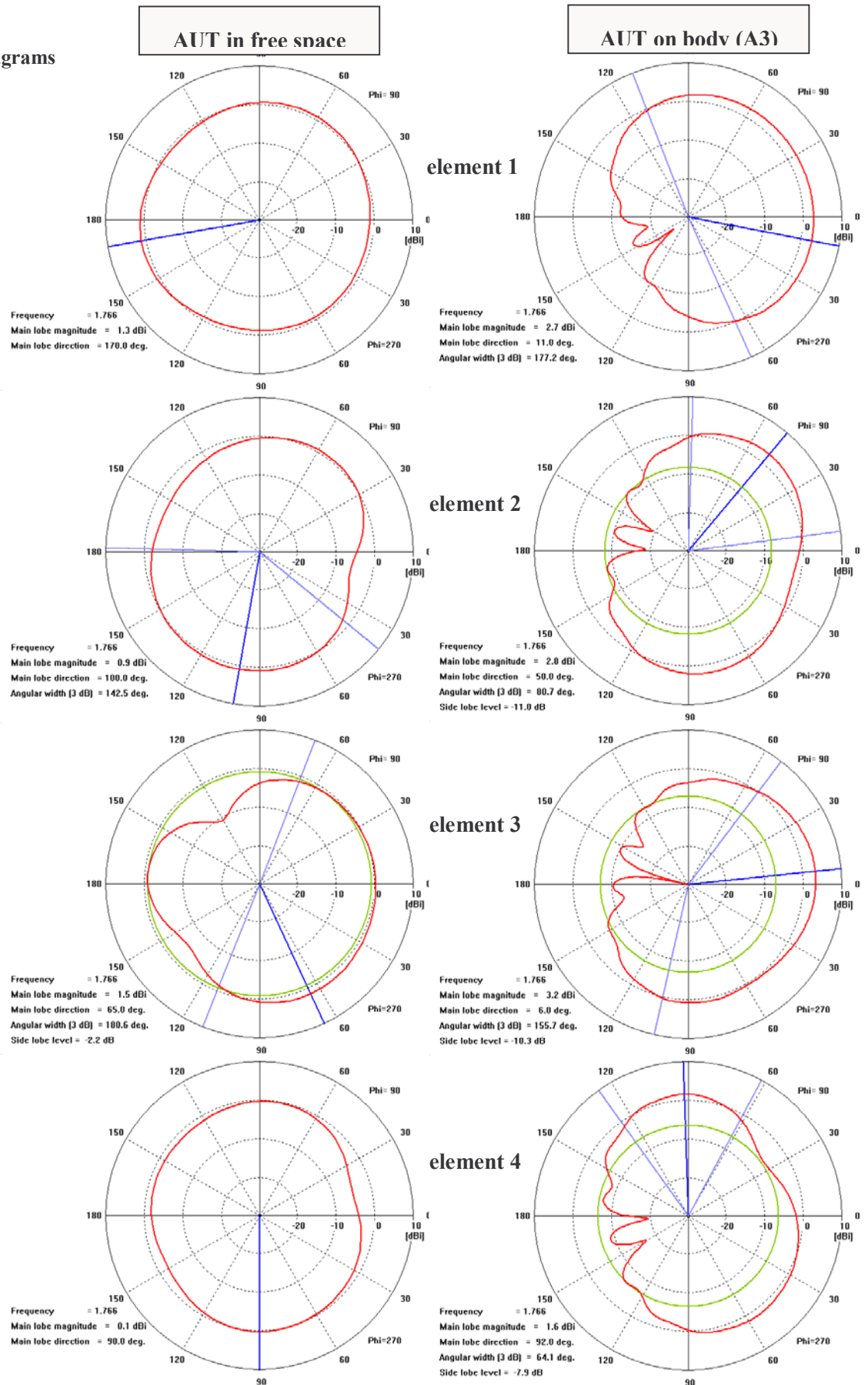
Fig. 40. Model of AUT on user's body (test case A3)

Simulations include,

- The **radiation diagrams** (directivity) for each array element,
- the **reflection coefficients** (S_{ii}) for each array element and
- the **mutual impedance matrix** between the array elements.

In Fig. 41, the radiation diagrams of the four elements, derived from the free space model (test case A1) are presented together with the corresponding radiation diagrams for the case A3 ("pocket position"). It is obvious that the user's body significantly affects the radiation diagram, especially in the direction towards the body (theta = 180 degrees)

Fig. 41 Radiation diagrams



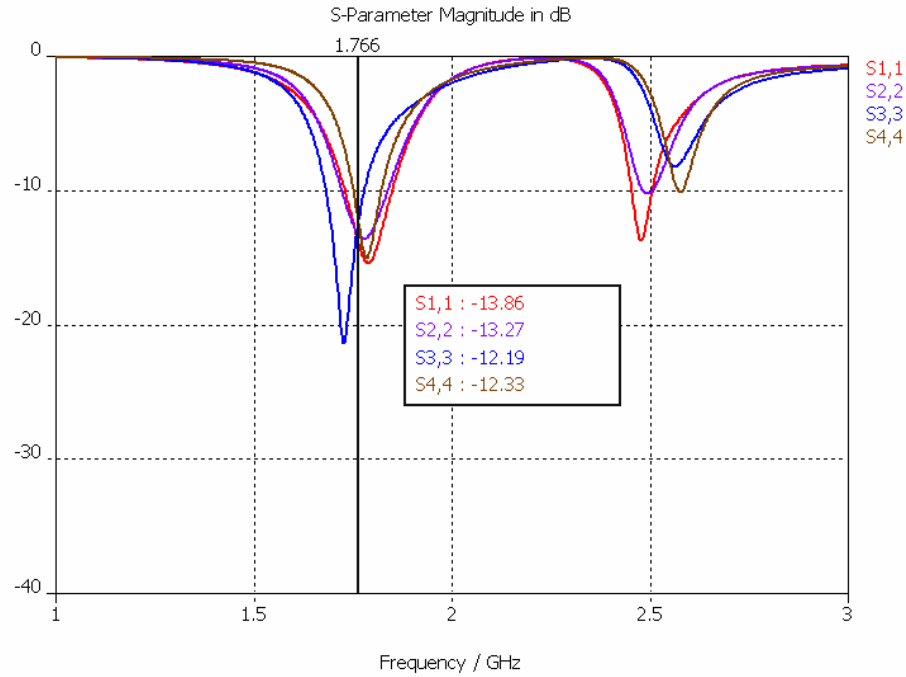


Fig. 43. Reflection coefficients (Sii) (test case A3)

The **Mutual impedance matrix** for the A3 test case is the following:

$$Z_{matrix} = \begin{bmatrix} 87.95 - j8.051 & 35.52 - j16.55 & 10.79 - j4.584 & 30.89 - j11.87 \\ 35.54 - j16.61 & 89.55 - j12.01 & 39.22 - j15.92 & 16.75 - j17.18 \\ 10.78 - j4.606 & 39.21 - j15.91 & 46.07 + j13.02 & 21.9 + j5.837 \\ 30.9 - j11.87 & 16.77 - j17.13 & 21.92 + j5.873 & 48.63 - j22.24 \end{bmatrix}$$

4.3 Results

The influence of the hand (referring to the S_{ii} parameter and the radiation diagram) is stronger on the elements that are closer to the hand (3, 4). There are no significant differences between the results for test cases A2a and A2b. Therefore we propose to use the homogeneous hand model, which requires less "run time". For the running of the CST models we have used a PC P4 @ 3.2 GHz with 2Gbyte RAM. The total run time for the A2a model was about 12.5 hours and for A2b model it was 16.5 hours.

Comparing the radiation diagrams in the cases A1, A2 and A3 the result is that the influence of the human body in the "pocket position" is much stronger than that of the hand alone in the "multimedia viewing position".

5 Conclusion and Discussion

We have evaluated the MIMO performance of a compact antenna array and a reference monopole array using three different methods. In all three cases, the major difference between the performance of the arrays is the lower radiation efficiency of the compact array. However, the difference in theoretical capacity is small, typically less than 10%.

Furthermore, we have studied the effect on the performance of the compact array when it is placed in the vicinity of the human body. This has been done using numerical simulations.

The analysis of the channel measurement data will continue in ACE-2. We also aim to present measurement results for the compact array in the vicinity of the human body.

References by members of ACE

- [1] Waldschmidt, C.; Schulteis, S.; Wiesbeck, W., "Complete RF system model for analysis of compact MIMO arrays," *IEEE Transactions on Vehicular Technology*, vol.53, no.3pp. 579- 586, May 2004
- [2] Kalliola, K.; Sulonen, K.; Laitinen, H.; Kivekas, O.; Krogerus, J.; Vainikainen, P., "Angular power distribution and mean effective gain of mobile antenna in different propagation environments," *IEEE Transactions on Vehicular Technology*, vol.51, no.5pp. 823- 838, Sep 2002
- [3] Gonzalez, A.N.; Lindmark, B., "The Effect of Antenna Orientation and Polarization on MIMO Capacity," *2005 IEEE Antennas and Propagation Society International Symposium*, , vol.3B, no.pp. 434- 437, 03-08 July 2005.
- [4] B. Lindmark, "Capacity of a 2 x 2 MIMO Antenna System with Mutual Coupling Losses, in *IEEE Antennas and Propagation Society International Symposium*, Monterey, CA, USA, June 2004.
- [5] Martínez-Vásquez and Oliver Litschke, "PMCIA Multi-Standard Antenna for Laptops", Presented at Joint COST 273/284 Workshop on Antennas and Related System Aspects in Wireless Communications, Gothenburg, Sweden, June 2004.
- [6] P.-S. Kildal and K. Rosengren, "Correlation and capacity of MIMO systems and mutual coupling, radiation efficiency and diversity gain of their antennas: Simulations and measurements in reverberation chamber", *IEEE Comm. Magazine*, vol. 42, no. 12, pp. 102-112, Dec. 2004.
- [7] K. Rosengren and P.-S. Kildal, "Radiation efficiency, correlation, diversity gain and capacity of a six-monopole antenna array for a MIMO system: theory, simulation and measurement in reverberation chamber", *IEEE Proceedings - Microwaves, Antennas and Propagation*, vol. 152, no. 1, pp. 7-16, Feb. 2005.
- [8] Sulonen, K.; Suvikunnas, P.; Vuokko, L.; Kivinen, J.; Vainikainen, P., "Comparison of MIMO antenna configurations in picocell and microcell environments," *Selected Areas in Communications, IEEE Journal on* , vol.21, no.5pp. 703- 712, June 2003
- [9] Outi Kivekäs, Jani Ollikainen, Tuukka Lehtiniemi, and Pertti Vainikainen, "Bandwidth, SAR, and Efficiency of Internal Mobile Phone Antennas", *IEEE TRANS. ON ELECTROMAGNETIC COMPATIBILITY*, VOL. 46, NO. 1, FEB 2004 pages 71-86.
- [10] P Zetterberg, "Wireless Development Laboratory (WIDELAB) Equipment Base", Technical Report, Department of Signals, Sensors and Systems, Royal Institute of Technology, IR-S3-SB-0316. Available from www.s3.kth.se/cgi-bin/signal/getreports.cgi.
- [11] P Zetterberg, "MUMS Documentation", Technical Report, Department of Signals, Sensors and Systems, Royal Institute of Technology, IR-S3-SB-0403, Available on from www.s3.kth.se/cgi-bin/signal/getreports.cgi.

Other References

- [12] Paulraj, A.J.; Gore, D.A.; Nabar, R.U.; Bölcskei, H., "An overview of MIMO communications - a key to gigabit wireless," *Proceedings of the IEEE* , vol.92, no.2pp. 198- 218, Feb 2004
- [13] A.C. Ludwig, "Mutual Coupling, Gain, and Directivity of an Array of Two Identical Antennas", *IEEE Trans. Antennas Propagat.*, Vol. AP-24, pp. 837-841, Nov. 1976.
- [14] T. Svantesson and A. Ranheim, "Mutual Coupling Effects on the Capacity of Multielement Antenna Systems", in *Proceedings IEEE ICASP '01*, vol. 4, pp. 2485-2488, 2001.
- [15] J.W. Wallace and M.A. Jensen, "Mutual Coupling in MIMO Wireless Systems: A Rigorous Network Theory Analysis", *IEEE Transactions on Wireless Communications*, Vol. 3, No. 4, July 2004.
- [16] P. Kyritsi, D.C. Cox, R.A. Valenzuela, and P.W. Wolniansky, "Effect of Polarization on the Capacity of a Multiple Element System in an Indoor Environment", *IEEE Journal of Selected Areas in Communications*, Vol. 20, No. 6, August 2002.
- [17] R. Vaughan, and J. Bach Andersen, "Antenna Diversity in Mobile Communications", *IEEE Trans. Veh. Technol.*, vol. VT-36, 99. 149-172, Nov. 1987.
- [18] A. Hirata and T. Shiozawa, "Correlation of maximum temperature increase and peak SAR in the human head due to handset antennas", *IEEE Transactions on Microwave Theory and Techniques*, v. 51, no. 7, p 1834-41, July 2003.
- [19] C. Braun, G. Engblom, C. Beckman, "Evaluation of antenna diversity performance for mobile handsets using 3-D measurement data", *IEEE Trans. Antennas Propagat.*, vol. 47, no. 11, p 1736-8, Nov. 1999.
- [20] C. Braun, M. Nilsson, and R.D. Murch, "Measurement of the interference rejection capability of smart antennas on mobile telephones", *IEEE 49th Vehicular Technology Conference*, pt. 2, p 1068-73 vol.2, 1999.

- [21] Duixian Liu, E. Flint, B. Gaucher, “Integrated Laptop Antennas - Design and Evaluation”, IEEE Antennas and Propagation Society International Symposium, pt. 4, p 56-9 vol.4, 2002.
- [22] M. Ali, M. Okoniewski, M.A. Stuchly, S.S.A. Stuchly, “Dual-frequency strip-sleeve monopole antenna for a laptop computer”, IEEE Antennas and Propagation Society International Symposium. 1998 Digest, pt. 2, p 794-7, vol.2, 1998.
- [23] Martínez-Vásquez and Oliver Litschke, “PMCIA Multi-Standard Antenna for Laptops”, Presented at Joint COST 273/284 Workshop on Antennas and Related System Aspects in Wireless Communications, Gothenburg, Sweden, June 2004.
- [24] M.A. Beach, M. Hunukumbure, C. Williams, G.S. Hilton, P.R. Rogers, M. Capstick, and B. Kemp, “An Experimental Evaluation of Three Candidate MIMO Array Designs for PDA Devices”, Presented at Joint COST 273/284 Workshop on Antennas and Related System Aspects in Wireless Communications, Gothenburg, Sweden, June 2004.
- [25] R. N. Simons, D. Chun, and L. P. B. Katehi, “Reconfigurable array antenna using microelectromechanical systems (MEMS) actuators,” in IEEE Antennas and Propagation Society International Symposium, vol. 3, 2001, pp. 674–677.
- [26] S. Xiao, B.-Z. Wang, and X.-S. Yang, “A novel frequency reconfigurable patch antenna,” in Microwave and Optical Technology Letters, vol. 1, 2003, pp. 295–297.
- [27] G. Huff, J. Feng, S. Zhang, and J. Bernhard, “A novel radiation pattern and frequency reconfigurable single turn square spiral microstrip antenna,” in IEEE Microwave and Wireless Components Letters, vol. 13, 2003, pp. 57–59.
- [28] W. H. Weedon, W. J. Payne, and G. M. Rebeiz, “MEMS-switched reconfigurable antennas,” in IEEE Antennas and Propagation Society International Symposium, 2001, pp. 654–657.
- [29] F. Yang and Y. Rahmat-Samii, “A reconfigurable patch antenna using switchable slots for circular polarization diversity,” in IEEE Microwave and Wireless Components Letters, vol. 12, 2002, pp. 96–98.
- [30] R.N. Simons, D. Chun, and L. P. B. Katehi, “Polarization reconfigurable patch antenna using microelectromechanical systems (MEMS) actuators,” in IEEE Antennas and Propagation Society International Symposium, vol. 2, 2002, pp. 6–9.
- [31] Hong-Twu Chen, Kin-Lu Wong, and Tzung-Wern Chiou, “PIFA With a Meandered and Folded Patch for the Dual-Band Mobile Phone Application”, IEEE Trans. Antennas propagate., vol. 51, no. 9, Sept. 2003.
- [32] Outi Kivekäs, Jani Ollikainen, Tuukka Lehtiniemi, and Pertti Vainikainen, “Bandwidth, SAR, and Efficiency of Internal Mobile Phone Antennas”, IEEE TRANS. ON ELECTROMAGNETIC COMPATIBILITY, VOL. 46, NO. 1, FEB 2004 pages 71-86.
- [33] ETSI Technical Report 273-7, February 1998, “Electromagnetic compatibility and Radio spectrum Matters (ERM); Improvement of radiated methods of measurement (using test sites) and evaluation of the corresponding measurement uncertainties; Part 7: Artificial human beings.

Acronyms/Terminology

AUT	Antenna Under Test
CAD	Computer Added Design
CSI	Channel State Information
MIMO	Multiple Input Multiple Output
PIFA	Planar Inverted F Antenna
REF	Reference antenna
SNR	Signal to Noise Ratio
WLAN	Wireless Local Area Network